Title: COVID-19 during pregnancy alters circulating extracellular vesicle cargo and their effects on trophoblast

Authors: Thea N. Golden[1,2*], Sneha Mani[1,2], Lauren Anton[1,2], Colin C. Conine[2,3,4,5,6,7], Rebecca L. Linn[8], Rita Leite[1,2], Brett A. Kaufman[9], Monica Mainigi[1,2], Natalie A. Trigg[7], Annette Wilson[9], Jerome F. Strauss III[1,2], Samuel Parry[1,2], and Rebecca A. Simmons[2,6,7]

Affiliations:

[1]Department of Obstetrics and Gynecology, Perelman School of Medicine at the University of Pennsylvania; Philadelphia, USA.

[2]Center for Research on Reproduction and Women's Health, University of Pennsylvania; Philadelphia, USA.

[3]Department of Genetics, Perelman School of Medicine at the University of Pennsylvania; Philadelphia, USA.

[4]Epigenetics Institute, Perelman School of Medicine at the University of Pennsylvania; Philadelphia, USA.

[5]Institute for Regenerative Medicine, Perelman School of Medicine at the University of Pennsylvania; Philadelphia, USA.

[6]Department of Pediatrics, Perelman School of Medicine at the University of Pennsylvania; Philadelphia, USA.

[7]Department of Neonatology, Children's Hospital of Philadelphia, Philadelphia, USA.

[8]Department of Pathology and Laboratory Medicine, Children's Hospital of Philadelphia; Philadelphia, USA.

[9]Department of Medicine, University of Pittsburgh; Pittsburgh, USA.

*Corresponding author. Email: goldent@pennmedicine.upenn.edu

One Sentence Summary: Circulating extracellular vesicles are altered by COVID-19 during pregnancy and contribute to placental dysfunction.

Abstract:

SARS-CoV-2 infection and the resulting coronavirus disease (COVID-19) complicate pregnancies as the result of placental dysfunction which increases the risk of adverse pregnancy outcomes. While abnormal placental pathology resulting from COVID-19 is common, direct infection of the placenta is rare. This suggests maternal response to infection is responsible for placental dysfunction. We hypothesized that maternal circulating extracellular vesicles (EVs) are altered by COVID-19 during pregnancy and contribute to placental dysfunction. To examine this, we characterized maternal circulating EVs from pregnancies complicated by COVID-19 and tested their functional effect on trophoblast cells *in vitro*. We found the timing of infection is a major determinant of the effect of COVID-19 on circulating EVs. Additionally, we found differentially expressed EV mRNA cargo in COVID-19 groups compared to Controls that regulates the differential gene expression induced by COVID-19 in the placenta. *In vitro* exposure of trophoblasts to EVs isolated from patients with an active infection, but not EVs isolated from Controls, reduced key trophoblast functions including hormone production and invasion. This demonstrates circulating EVs from subjects with an active infection disrupt vital trophoblast function. This study determined that COVID-19 has a long-lasting effect on circulating EVs and circulating EVs are likely to participate in the placental dysfunction induced by COVID-19.

INTRODUCTION

Maternal SARS-CoV-2 infection and the resulting coronavirus disease (COVID-19) is associated with an increased risk of pregnancy complications including preterm birth, hypertensive disorders of pregnancy, fetal growth restriction, and pregnancy loss (*1-5*). Placental dysfunction is known to contribute to these complications, and placental pathology, including vasculopathies and inflammation, is frequently reported following an acute or even resolved infection during pregnancy (*6-11*). This suggests COVID-19 has a long-lasting effect on maternal pregnancy via placental pathology. Despite extensive reports of placental pathology observations following COVID-19, little is known about the underlying mechanisms contributing to placental dysfunction and the potentially related, subsequent pregnancy complications. Direct infection of the placenta is rare which suggests placental dysfunction is caused by the maternal response to SARS-CoV-2 infection (*10, 12, 13*).

Circulating extracellular vesicles (EVs) are known to be altered by SARS-CoV-2 infection and contribute to COVID-19 induced organ damage and dysfunction.(*14-19*) EVs are a means of cell-to-cell communication because they carry bioactive cargo that elicits signaling events in recipient cells. Circulating EVs constitute a diverse population of vesicles carrying bioactive cargo that arise from many cellular sources. Two pathways of biogenesis create what is commonly referred to as large and small EVs (LEVs and SEVs). When compared with non-infected patients, EV cargo in patients with COVID-19 is altered, which elicits downstream effects such as coagulopathy (*20-25*) and inflammation (*15, 16, 22, 23, 26, 27*). Tissue factor abundance in EVs is also increased in COVID-19 and correlates with inflammation and disease severity (*14, 17-19*). These examples demonstrate the influence that circulating EVs have on the systemic response to COVID-19, thereby leading to distal organ dysfunction.

During normal pregnancy, the placenta releases EVs into the maternal circulation (*28-30*). Placental-derived EVs promote maternal adaptation to support a healthy pregnancy including a shift in the maternal immune system to a tolerant state (*31, 32*) as well as angiogenesis promotion (*33*). Placental-derived EVs also affect trophoblast function via autocrine and paracrine signaling. Trophoblasts are a specialized cell type of the placenta that are responsible for invasion into maternal tissue to anchor the placenta, vasculature remodeling for adequate placental blood flow, and hormone production for maternal and fetal signaling. Perturbation of normal trophoblast function, as caused by altered EV signaling, underlies the placental dysfunction that contributes to many pregnancy complications (*34-41*). Importantly, EV characteristics such as number and cargo are altered in multiple pregnancy complications (*42*).

We hypothesized that COVID-19 induces placental morphologic and transcriptomic changes and alters EV characteristics which have functional consequences in the placenta. Similar to previous studies, COVID-19 during pregnancy induced marked placental histologic and transcriptomic changes which were dependent on the gestational timing of COVID-19. Importantly, we found that COVID-19 altered EV cargo and trophoblast exposure to EVs resulted in marked dysfunction including reduced cell invasion and hormone production.

RESULTS

Pregnancy outcomes following active and resolved SARS-CoV-2 infection

Subjects were enrolled at the time of delivery between July 2020-August 2022. Controls had no known SARS-CoV-2 infection during pregnancy. COVID-19 cases were divided based on the gestational timing of infection and either had a resolved infection that occurred in the 1st, 2nd, or 3rd trimester (R1, R2, R3), or had an active infection at the time of delivery (AI) (Table 1).

There were no significant differences in maternal age between groups, but there were significantly more Black subjects with an infection in the third trimester (resolved or active) compared to Controls. Subjects with an infection in the third trimester also had a lower gestational age at delivery than Controls (Table 1). Despite testing positive for SARS-CoV-2 at the time of delivery, the AI group had a higher incidence of asymptomatic infection than those with a resolved infection ($p<0.0001$).

Multiple studies have shown that SARS-CoV-2 infection during pregnancy is associated with adverse pregnancy outcomes. However, to date, no study has examined the relationship between the timing of infection and pregnancy complications in a single cohort. We found that the type of adverse outcome differed depending on the gestational timing of infection. The incidence of gestational hypertension was increased in R1, whereas spontaneous preterm birth was increased in R2. Preeclampsia and medically indicated preterm birth were increased in R3 and AI compared to Controls (Table 1).

Placental pathology in COVID-19

Abnormal placental pathology is commonly reported in patients with active and resolved SARS-CoV-2 infections (*7*), however, there has yet to be a comprehensive assessment of placentas following maternal infection at various gestational ages. Similar to previous reports (*6-11*), we found either maternal or fetal vascular malperfusion (MVM &FVM) lesions were increased by COVID-19 (Table 1). Interestingly, high-grade MVM and perivillous fibrin deposition was increased in subjects with a resolved infection that occurred in the second or third trimester, but not the first trimester or with an active infection. This suggests that it takes a substantial amount of time for the placenta to recover from COVID-19. Alternatively, it is possible that the first trimester placenta is more resilient. The lack of high-grade MVM and

perivillous fibrin deposition in placenta collected from subjects with an active infection suggests these particular lesions take many weeks to manifest.

Timing of COVID-19 impacts the placental transcriptome

To gain insight into potential novel pathways that might be disrupted by COVID-19 infection during pregnancy, we sequenced the transcriptome of the placenta. Multiple genes were differentially expressed in COVID-19 groups compared to Controls (Supplemental Table 1). Not surprisingly, the transcriptome was most altered in placenta from pregnancies complicated by an active infection (Figure 1). When comparing the Control placenta to 3rd trimester resolved infection and active infection, DEGs were mostly downregulated (Supplemental Table 1). Interestingly, prostaglandin E receptor 2 (PTGER2) is decreased in Control placenta compared to AI. PTGER2 encodes for a prostaglandin receptor and downstream signaling regulates trophoblast behavior. In contrast, differentially expressed genes were predominately upregulated in Control placentas compared to R1. One of the few differentially expressed genes upregulated in R1 placenta encodes for a mitochondrial protein (*MTARC2).* Finally, there were a few differences between the R2 and control placentas. Interestingly there was overlap in DEGs in placentas in the resolved infection groups and the actively infected group (Supplemental Table 1). This suggests that COVID-19 induces permanent changes in gene expression in the placenta even when the infection is remote to delivery.

We used Ingenuity Pathway Analysis (IPA) to identify disrupted canonical pathways (Table 2). Several common pathways were altered in placenta from COVID-19 groups, including fibrosis and many inflammatory and immune regulating pathways. Thus, despite the long period of time following the resolution of maternal SARS-CoV-2 infection, the placenta has evidence of persistent inflammation and fibrosis.

Sustained effects on circulating EVs following COVID-19 in early pregnancy

EVs mediate cellular communication and play a fundamental role in the maintenance of tissue homeostasis and pathogenesis in several diseases. As discussed above, SARS-CoV-2 rarely infects the placenta and maternal circulating EVs are likely to play a role in mediating placental dysfunction. Therefore, we characterized EVs isolated from maternal plasma collected at delivery to determine if the EV profile was altered by COVID-19. The presence of large (LEV) and small EVs (SEV) in isolated particles was confirmed by morphological assessment of electron microscopy images (Figure 2A). Isolated LEVs and SEVs also had the expected size distribution of EVs (Figure 2B). Finally, the expression of the EV related tetraspanin, Cd9, was abundant in isolated particles (Figure 2C).

EV characteristics, including the concentration and size distribution, revealed persistent alterations in patients with a resolved infection. We found the diameter of SEVs was significantly increased in resolved infections compared to Controls, 108.7 vs. 117.2nm ($p=0.023$), but the difference in concentration was not significantly different, $2.15x10^8$ vs. 1.56 $x10^8$ EVs/uL plasma ($p=0.074$). When resolved infections were further divided by trimester, we found SEVs isolated from R2 circulation have an increased diameter and reduced concentration, but SEVs isolated from R1 and R3 were not different from Controls (Figure 3 C&D). In LEVs isolated from R2, we also found a decrease in their diameter but no change in the number of LEVs (Figure 3B). The uniquely persistent effect of COVID-19 on the concentration and size of circulating EVs in the second trimester may point to a particularly susceptible pregnancy-related pathway in this gestational window.

Altered cell of origin of EVs in patients with COVID-19 in early pregnancy

Characterizing the source of circulating EVs provides biological information about both the tissue and cell-type of origin as well as its functional state. We therefore used flow cytometry to detect cell-specific vesicle membrane protein expression and identified the relative contribution of each EV tissue-cellular source. The studied cells included those of maternal endothelial cells (Cd31+ Cd34-), fetal endothelial cells (Cd31+ Cd34+), platelets (Cd41a+), immune cells (Cd45+), and trophoblasts (PLAP+) (Figure 4).

Trophoblast derived PLAP+ EVs comprised the largest proportion of circulating LEVs (Figure 4A). The percentage of PLAP+ EVs was increased in the circulation of R2 compared to Controls suggesting the placenta secreted more LEVs into circulation. Interestingly, we found a subset of endothelial-derived EVs that also express Cd34, suggesting that these EVs originated from fetal endothelial cells (*43*). Fetal endothelial cell-derived LEVs (Cd34+ Cd31+) were also elevated in R1 and R2 compared to Controls. Surprisingly, the percentage of SEVs from the placenta was not altered by COVID-19. In fact, there was no difference in the percentage of SEVs from any cell type measured. This suggests that placenta-derived LEVs, but not SEVs, were persistently altered by COVID-19 in early pregnancy.

EVs alter trophoblast function *in vitro*

The placenta is made up of two main functional cell types- syncytiotrophoblasts, which are responsible for hormone production, and extravillous trophoblasts, which invade deep into the uterus to anchor the placenta and enable blood and nutrient flow to the fetus. EV signaling is known to influence trophoblast function (*44*). We tested the capacity for circulating EVs isolated from subjects with an active infection or Controls to alter the function of both major trophoblast cell types. To study syncytiotrophoblasts, we used the BeWo choriocarinoma cell line which is an established cell line commonly used to study syncytiotrophoblast behavior.

After the addition of the cAMP producer forskolin, BeWo cells mimic syncytiotrophoblasts morphologically via syncytialization and functionally through the production of hormones such as hCG and progesterone. To assess extravillous trophoblasts (EVT) behavior, we used primary EVTs isolated from first trimester placenta and quantified the extent of invasion using an invasion assay. We chose to focus our *in vitro* experiments on EVs isolated from subjects with an active infection compared to Controls because the changes in placental pathology and the number of differentially expressed genes in the placenta was highest in AI cases compared to Controls.

Syncytiotrophoblast hormone production is vital to maintain a healthy pregnancy. The ratio of hCG to progesterone in the media was reduced following exposure to AI EVs compared to Control EVs (Figure 5A). A reduction of the ratio of hCG to progesterone indicates specific pathways related to hormone production were disrupted instead of reduced cellular activity which would result in an overall decrease in both levels and therefore a similar ratio. Altered pathways may include reduced transcription or translation which are key to hCG production or altered mitochondrial function which is key to progesterone synthesis. This demonstrates that AI EVs, but not Control EVs, disrupt trophoblast hormone production which may have profound effects on pregnancy maintenance.

Remarkably, extravillous trophoblast invasion was also reduced by exposure to AI EVs compared to Control EVs (Figure 5B). EVT invasion is vital to anchor the placenta to the maternal uterus and failure to appropriately do so increases the risk of preeclampsia, intrauterine growth restriction, and fetal loss.(*45, 46*) This extraordinary finding suggests that circulating EVs from pregnancies complicated by an active infection have the potential to directly reduce trophoblast invasion.

To identify novel pathways that may contribute to trophoblast dysfunction, we measured the BeWo transcriptome following EV exposure. AI EVs significantly altered gene expression in BeWo cells compared to Control EVs. 65 DEGs were identified, and the top differentially expressed genes encode for histone proteins (Table 3). This demonstrates a disruption of DNA packaging and transcription in trophoblasts exposed to AI EVs compared to Control EVs. Moreover, a top canonical pathway identified by IPA is related to cellular transcription (*Transcriptional Regulatory Network in Embryonic Stem Cells*) (Table 4) (*47*).

EV RNA cargo was altered in patients who experienced COVID-19 during pregnancy

Prior studies have shown that EVs carry bioactive cargo. Here, we sought to determine the cellular signaling effect of EV cargo on trophoblasts. Nucleic acids are the most commonly studied EV cargo, and small RNAs, particularly micro RNAs, are the most abundant (*48*). However, longer RNAs, such as messenger RNAs (mRNAs), have also been found and have not been widely studied. mRNAs encapsulated within EVs have been shown to be transferred to recipient cells and translated into proteins, altering the behavior of the cells (*49-57*). Therefore, we profiled the mRNA cargo content in circulating SEVs and LEVs to determine if there were differences dependent on the gestational timing of COVID-19. We sequenced an average of 2,946 transcripts in LEVs and 1,947 transcripts in SEVs.

We identified multiple uniquely expressed genes in EVs between the groups. Transcripts expressed by LEVs isolated from COVID-19 groups but absent in Controls include *YY1AP1*, *MOSPDI, RYBP*, and *H1-4* (Table 5). The proteins these transcripts encode are related to transcription, except for *HI-4* which has an unknown cellular function. In SEVs, *MYL4 and C18orf32,* CAPG, and CTSS COVID-19 groups, but not in Controls (Table 6). These transcripts encode for motor and immune proteins. Many other genes were uniquely detected in LEVs and

SEVs isolated from individual COVID-19 groups (Table 5&6). The unique expression of these transcripts suggests that COVID-19 induces upregulation of these transcripts making them more available for EV packaging or increased specific transcript loading into EVs.

EVs isolated from Controls carry several interesting transcripts that were uniquely expressed in Controls, i.e. not in COVID-19 groups. LEVs isolated from COVID-19 groups are missing *APBA3*, *MTSS*, *FCF1*, *PSG2, LOC100128233*, *PHOSPHO2* and *THOC3* which are abundant in Control EVs (Figure 6A). These transcripts encode for proteins that were involved in various cellular functions. In contrast, only a few transcripts were unique to Controls in SEVs. These include *PYCR2, SCGB1C1*, and *CD300L4* (Figure 6B). *PYCR2* encodes for a cellular metabolism protein, *CD300L4* encodes for an immune regulating protein, and the protein function of *SCGB1C1* is unknown. Numerous other abundant Control transcripts were absent in individual COVID-19 groups and the corresponding expression in the other COVID-19 groups was commonly downregulated (Figure 6). The loss of these physiologically expressed genes in EVs isolated from COVID-19 groups suggest COVID-19 disrupts normal EV cargo.

The transcripts carried by EVs reflect the activity of the secreting cell. While the individual genes identified in LEVs and SEVs differ, the cellular functions of these genes often overlapped (Table 5&6, Figure 6). For example, large and small EVs isolated from R2 carried transcripts that control cell signaling, gene expression, immune regulation, and metabolism. Other overlapping cellular activities of interest were proliferation, apoptosis, invasion, ubiquitination, platelet function, and vesicle formation.

Many transcripts that were identified in LEVs and SEVs have been shown to be highly expressed in trophoblasts and previously reported to increase with gestation (Table 5&6 and Figure 6). Interestingly, LEV expression of *THOC3*, a highly expressed transcript in

trophoblasts, was abundant in Control LEVs but lowly expressed or absent in the COVID-19 groups. In addition, LEVs carry a different highly expressed trophoblast transcript, *RYBP*, in COVID-19 groups, but this transcript is absent in Controls. Both genes encode for transcription regulating proteins. Several of the uniquely expressed genes in EVs isolated from COVID-19 groups have been previously reported to be associated with adverse pregnancy outcomes, including fetal growth restriction, preeclampsia, gestational hypertension, and preterm birth (Supplemental Table 2). The number of these genes was highest in AI EVs, but also abundant in EVs isolated from subjects with resolved infections (Figure 7). Interestingly, eleven transcripts that have been implicated in preeclampsia were differentially expressed by AI EVs compared to Control EVs. Moreover, two transcripts associated with preterm birth were uniquely carried by R2 but not Control EVs. This suggests that there may be a shared etiology of these pregnancy complications because the incidence of these complications was also increased in these COVID-19 groups.

Regulators of COVID-19 induced differential gene expression in the placenta are in circulating EVs

We used IPA to identify upstream regulators of gene expression that were carried by circulating EVs in COVID-19 groups and determined whether their downstream target genes were differentially expressed in placenta. Surprisingly, we found many upstream regulators were carried by circulating EVs and were differentially expressed between the COVID-19 group and the Controls (Table 7). For example, Jun proto-oncogene B (*JUNB*) mRNA levels were increased in LEVs from R1 compared to Controls (FC=-2.25, p=0.01) and JUN signaling was altered in R1 placenta compared to Controls. Likewise, interleukin 1 beta (*IL1β)* mRNA was decreased in R3 LEVs compared to Controls (FC=1.85, p=0.07) and IL1β signaling was also

altered in R3 placenta compared to Controls. Finally, estrogen receptor 1 (*ESR1*) mRNA was decreased in R3 SEVs compared to controls (FC=6.99, p=0.13) and ESR1 signaling was predicted to regulate differential gene expression in R3 placenta compared to Controls. These examples exemplify potential EV driven signaling that cause differential gene expression in the placenta.

mtDNA was abundant in LEVs and increased following COVID-19 in early pregnancy

Analysis of the placental transcriptome following COVID-19 identified differentially expressed genes indicative of mitochondrial dysfunction. To determine if EVs were enriched in mitochondrial cargo, we measured mitochondrial DNA (mtDNA) in circulating EVs (Figure 8A &D) and found mtDNA was more abundant in large than small EVs. Also, the abundance of mtDNA in LEVs, but not SEVs, inversely correlated with the gestational timing of infection (Figure 8 B&D). This suggests that the mitochondrial function of cells producing LEVs were disrupted by COVID-19.

DISCUSSION

The long-term effects of COVID-19 during pregnancy have not yet been elucidated. Previous studies, and what is reported here, show that the placenta is persistently damaged, and the likelihood of adverse pregnancy outcomes increases in patients with a pregnancy complicated by SARS-CoV-2 infection. Here, we have begun to dissect out the mechanisms underlying the observed placenta pathology and dysfunction. Importantly for the first time, we demonstrate that circulating EVs from COVID-19 affected pregnancies 1) have a detrimental effect on trophoblast function, including hormone production and invasion, *in vitro*; 2) are persistently altered after SARS-CoV-2 infection; and 3) carry cargo that has been previously associated with adverse pregnancy outcomes.

Trophoblast dysfunction following exposure to EVs isolated from subjects with an active SARS-CoV-2 infection *in vitro* provides evidence that circulating EVs contribute to the resulting placental pathology. We chose to focus our *in vitro* trophoblast experiments on the response to EVs isolated from subjects with an active infection because the magnitude of alteration to the placental transcriptome was greater compared to those placentas from resolved infections. Analysis of the BeWo transcriptome after AI EV exposure showed that top differentially expressed genes encode histone proteins, suggesting alterations in chromatin packaging. Disrupted DNA replication may be the underlying mechanism leading to reduced hormone production following the same exposure. Trophoblast hormone production is key to maintaining a healthy pregnancy and altered levels are associated with pregnancy complications such as preeclampsia and fetal demise *in utero* (*58*). Reduced BeWo hormone production following exposure to AI EVs suggests a failure of the placenta to produce hormones in the presence of circulating EVs. Extravillous trophoblast invasion is key to implantation, and failure to appropriately invade is implicated in the pathogenesis of preeclampsia, fetal growth restriction, and preterm birth (*45, 46*). Therefore, the reduction of EVT invasion following exposure to AI EVs, suggests that EVs have the capacity to reduce invasion and impede placentation. Collectively, the effect of circulating EVs isolated from patients with an active infection on trophoblasts *in vitro* are profound and suggest AI EVs have the capacity to contribute to the placental pathology observed in pregnancies complicated by COVID-19.

Gestational age at the time of infection is a major determinant of COVID-19-induced changes in the profile of circulating EVs. If infected during the first or second trimester of pregnancy, trophoblast and fetal endothelial cell LEV numbers are increased and circulating LEVs carry more mtDNA. This suggests that mitochondrial function in the placenta in early

pregnancy is perturbed by COVID-19. Mitochondrial dysfunction is also reported in many organs following SARS-CoV-2 infection and is thought to contribute to cell death, inflammation, and cell injury (*59-63*). Appelman et al. recently reported persistent mitochondrial dysfunction in skeletal muscle long after the resolution of SARS-CoV-2 infection (*64*). Cells undergoing mitochondrial dysfunction release mtDNA. In support of this, Faizan et al. recently demonstrated that SARS-CoV-2 infected airway epithelial cells with mitochondrial dysfunction release mtDNA in EVs (*60*). Further, elevated circulating mtDNA, is well established in COVID-19 and correlates with severity and length of infection (*65-68*). Thus, our results suggest that abnormal mitochondria may also play a role in the pathogenesis of placental dysfunction in COVID-19 as we and others have shown.

Circulating EV cargo reflects the activity of the cells of origin. The transcripts carried by EVs encode genes related to inflammation, vasculopathies, bioenergetics, and cell death. These pathways are also evident in the transcriptome and histopathology of the placenta regardless of the timing of infection. Many of the transcripts carried by EVs are highly expressed by trophoblasts and have known roles in trophoblast function including cellular metabolism, transcription, and immune regulation. We also found that many of the transcripts in EVs from pregnancies complicated by COVID-19 are also implicated in adverse pregnancy outcomes including preterm birth, fetal growth restriction, gestational hypertension, and preeclampsia. This points to shared pathways of placental dysfunction induced by a distal SARS-CoV-2 infection.

EV cargo is selectively packaged and functionally active upon interaction with recipient cells. RNA is selectively incorporated into EVs and is biologically active in target cells (*48*). Mitochondrial DNA packaged in EVs can alter the recipient cell's mitochondrial function (*69-*

71). The capacity for EVs to elicit a functional response in recipient cells is illustrated by the trophoblast response to EVs isolated from patients with an active infection.

The overlap of uniquely expressed genes in EVs and the IPA predicted upstream regulators of the placental transcriptome suggests EV mRNA cargo may participate in altering the placental transcriptome. JUN signaling is altered in R1 placenta compared to Control placenta and *JUNB* mRNA is increased in Control LEVs compared to R1 LEVs. JUN proteins are important for placentation, and a loss of JUN signaling is implicated in preeclampsia (*72, 73*). Thus, low levels of JUNB in COVID-19 EVs may suggest placental dysfunction leading to the later development of preeclampsia, which is observed at higher rates in pregnancies complicated by COVID-19 (*74*). In R3, hormone receptor signaling is identified as a top canonical pathway and differentially expressed genes are regulated by ESR1. *ESR1* mRNA is abundant in SEVs isolated from Controls but not R3. ESR1 and other hormone receptor signaling is important for maintaining a healthy pregnancy and placental function. The presence of upstream regulators in circulating EVs suggest placental dysfunction may in fact be a result of EV cargo delivery.

Our study is limited by the number of symptomatic patients with an active infection at the time of delivery. Despite only 14% of patients experiencing COVID-19 related symptoms, the placenta had significant pathology and altered transcriptome, and there was an increase in the incidence of preeclampsia and medically indicated preterm birth in asymptomatic and symptomatic AI cases. Interestingly, EVs isolated from asymptomatic patients also had profound effects on trophoblasts *in vitro*. This suggests that we are underestimating the effect of a symptomatic active SARS-CoV-2 infection on circulating EVs and placental function.

Our study demonstrates the effect of maternal SARS-CoV-2 infection on circulating EVs and that EVs can contribute to placental pathology following COVID-19. This is the first study to analyze the effect of maternal circulating EVs on trophoblast function. The placental transcriptome and EV cargo reveal overlap in pathways that underlie pregnancy complications caused by maternal COVID-19 and other less well understood disorders. Future studies should test if the maternal circulating EVs in other pregnancy disorders contribute to placental dysfunction.

Figure 1. Differential gene expression in the placenta induced by COVID-19 during pregnancy. The number and direction of differentially expressed genes between Controls and resolved infections in the first trimester (R1), second trimester (R2), and third trimester (R3) and active infection (AI). (n=9-10/group)

Figure 2. Extracellular vesicles are isolated from the plasma by serial centrifugation. **(A)** Representative transmission electron microscope images demonstrated EV structure including a lipid membrane. **(B)** Nanotracking analysis was used to determine the size of particles in three control samples **(C)** Cd9 expression evaluated by immune-blotting was abundant in isolated particles in three control samples.

Figure 3. Circulating EVs were persistently altered in patients who experienced COVID-19 in the second trimester. **(A)** The number of LEVs in the circulation at the time of delivery (n=14-22/group). **(B)** The diameter of LEVs in the circulation (n=14-22/group). **(C)** The number of SEVs in the circulation at the time of delivery (n=14-22/group). **(D)** The diameter of SEVs in the circulation (n=14-22/group). All data are presented as mean ± SD. All analyses were performed by one-way ANOVA or the Kruskal-Wallis test, followed by post-hoc tests. Comparisons were made between Controls and resolved infection in the 1st trimester (R1), second trimester (R2), third trimester (R3), and active infection (AI).

Figure 4. COVID-19 in early to mid-pregnancy increased the contribution of endothelial cells and trophoblasts to the circulating LEVs. **(A)** Relative frequency of LEVs derived from endothelial cells, platelets, immune cells, and trophoblasts (n=11-16). **(B)** The relative frequency of SEVs derived from endothelial cells, platelets, immune cells, and trophoblasts (n=13-20/group). All data are represented as mean ± SD. All analyses were performed by one-way ANOVA or Kruskal-Wallis test, followed by post-hoc tests. Comparisons were made between

Controls and resolved infection in the 1st trimester (R1), second trimester (R2), third trimester (R3), and active infection (AI).

Figure 5. Trophoblast function was altered by exposure to EVs isolated from patients with an active infection (AI) compared to Controls. **(A)** Human chorionic gonadotropin (hCG) and progesterone were measured in the media of forskolin-treated (syncytialized) BeWo cells. The ratio of hCG to progesterone was normalized to hormone production by cells not exposed to EVs (noEVs). The results of two experiments (identified by symbol shape) are reported in A. (n=6-7/group, 2 experiments). **(B)** Extravillous trophoblasts (EVTs) were isolated from three placentae (identified by symbol shape) and exposed to Control or AI EVs (n=9-10/group, 3 experiments). Invasion was calculated and normalized to invasion of EVTs not exposed to EVs. All data are presented as mean ± SD. All analyses were performed by one-way ANOVA or Kruskal-Wallis test, followed by post-hoc tests.

Figure 6. Control EVs carried transcripts that were absent in COVID-19 groups. **(A&B)** Genes were identified as uniquely expressed in Controls if all comparison samples had no expression (gray bars). The expression of each COVID-19 group compared to Controls is shown in the heat map. The lower the expression in COVID-19 groups the darker the blue, and if expression was increased in a COVID-19 group compared to Controls it was colored red. The general cellular function of each gene is listed on the right. LEV transcripts are reported in (A) and SEV transcripts are reported in (B) (n=9-10/group). Comparisons were made between Controls and resolved infection in the 1st trimester (R1), second trimester (R2), third trimester (R3), and active infection (AI). Transcripts known to be highly expressed by trophoblasts are marked by (T).

Figure 7. Uniquely expressed genes associated with adverse pregnancy outcomes were expressed in EVs. The number of genes with previously reported altered expression in fetal

growth restriction (FGR), preeclampsia (PE), gestational hypertension (gHTN), and preterm birth (PTB) are quantified.

Figure 8. LEV abundance of mtDNA is inversely correlated with gestational timing of infection. **(A&C)** The amount of mtDNA in each LEV (A) and SEV (C) is reported for each group (n=13-20/group). Data are presented as mean ± SD and tested by ANOVA followed by post-hoc tests. Comparisons were made between Controls and resolved infection in the 1st trimester (R1), second trimester (R2), third trimester (R3), and active infection (AI). **(B&D)** The Pearson correlation between gestational age at infection and mtDNA content is reported for LEV (B) and SEV **(D)**.

MATERIALS AND METHODS

Patient Cohort

The COMET study was conducted at the Hospital of the University of Pennsylvania (HUP) with Institutional Review Board approval (IRB#843277). Subjects received a description of the study and signed an informed consent before enrollment. Subjects were enrolled at the time of delivery in the COMET study between April 2020-June 2022. Subjects were tested for a SARS-CoV-2 infection by nasopharyngeal polymerase chain reaction (PCR) upon admission to the labor and delivery unit at HUP. Subjects who tested positive at the time of delivery were enrolled in the active infection (AI) group. Those subjects who tested negative and had no known SARS-CoV-2 infection during their pregnancy were included as Controls. Subjects with a negative test at delivery and a history of SARS-CoV-2 infection, during their pregnancy and greater than 14 days before enrollment, were included in the resolved infection group (R). The gestational age of SARS-CoV-2 infection was calculated, and subjects were further divided into the trimester of

infection (resolved infection in the first trimester (R1), resolved infection in the second trimester (R2) and resolved infection in the third trimester (R3)).

Clinical and Demographic Data Collection

Clinical characteristics, such as maternal age, self-identified race, gestational age at infection, and pregnancy outcomes, were extracted from the medical record (Table 1).

The severity of COVID-19 disease was categorized based on the National Institute of Health and Society for Maternal-Fetal Medicine definitions: Asymptomatic infection are individuals who test positive but experience no symptoms. Symptomatic patients include all levels of illness (mild-critical).

Sample Collection

Placenta were collected at the time of delivery. All placentas were examined by the pathology department at the Hospital of the University of Pennsylvania (HUP). Placenta were reviewed following a systematic protocol which includes recording the trimmed placental weight, membrane insertion site, gross appearance, dimensions of the placental disc, and umbilical cord insertion, length, and diameter. Full thickness placental biopsies were collected and fixed in 10% formalin for histological assessment. Macroscopic and microscopic lesions were identified and classified according to the Amsterdam Placental Workshop Group 2014 classification (*75-77*). Placental biopsies were also collected and stored in Trizol for RNA sequencing.

Blood was collected at the time of delivery in an EDTA tube and spun at 1,000G for 10 minutes at room temperature to isolate plasma, which was aliquoted and stored at -80.

Placenta and BeWo RNA Isolation and Sequencing

Total RNA was isolated from placenta samples using Qiagen RNEasy Plus Mini Kits (Cat# 74134 Qiagen, Hilden, Germany). Total RNA was isolated from BeWo cells with the PicoPure RNA Isolation Kit (Cat# KIT0204 Applied Biosystems, Waltham, MA). Isolated RNA was sent to NovoGene for library preparation and sequencing.

RNA integrity and quantification was assessed using the RNA Nano 6000 Assay Kit of the Bioanalyzer 2100 System (Agilent Technologies, CA, USA). RNA purity was checked using a NanoPhotometer spectrophotometer (IMPLEN, CA, USA). A total of 1μg RNA per samples was used as input material for the RNA sample preparation. Sequencing libraries were generated using NEBNext Ultra RNA Library Prep Kit for Illumina (NEB, USA) following manufacturer recommendations, and index codes were added to identify samples. Clustering of the index-coded samples was performed on an Illumina Novaseq sequencer according to manufacturer's instructions. After cluster generation, libraries were sequenced, and pair-end reads were generated. Raw data (raw reads) of FASTQ format were processed through fastp. and clean data was obtained by removing reads containing adapter and poly-N sequences and reads with low quality. Pair-end clean reads were aligned to the GRCh38/hg38 reference genome using Spliced Transcripts Alignment to a Reference (STAR) software. FeatureCounts were used to count the read number mapped to each gene. Then RPKM of each gene was calculated based on the length of the gene and read count mapped to the gene. Differential gene expression between COVID-19 groups and Controls was tested by DESeq2 method. Differentially expressed genes were determined based on their adjusted p-value (<0.05) and >1.5-fold change. Functional analysis was conducted using Qiagen's ingenuity pathway analysis (IPA). Canonical pathways and upstream regulators with a p-value <0.05 were considered.

EV Isolation and Characterization

Serial centrifugation was utilized to isolate EVs from plasma. One mL of plasma was spun in an Eppendorf 5424 benchtop centrifuge at 2,000 x g for 10 minutes at 4°C. The supernatant was then spun at 20,000 x g for 30 minutes at 4°C. The pellet (LEVs) was washed in 1mL filtered PBS and spun again at 20,000 x g for 30 minutes at 4°C. The LEV pellet was resuspended in 100uL filtered PBS. The supernatant was spun by the Beckman Ultracentrifuge Optima Max TL using the TLA 120.2 rotor at 100,000 x g (48,000RPM) for 90 minutes at 4°C. The pellet (SEVs) was washed with 1mL filtered PBS and spun again at 100,000 x g (48,000RPM) for 90 minutes at 4°C. The SEV pellet was resuspended in 100uL filtered PBS.

EV isolation was confirmed by transmission electron microscopy, nanoparticle tracking, and protein measurement. Transmission electron microscopy images were generated and resulting images reviewed for the presence of EVs. EVs were analyzed by Particle Metrix Zetaview nanoparticle tracking. 11 fields were captured using the following parameters: sensitivity 80, frame rate 30, shutter 100, minimum brightness 1000, minimum area 10, trace length 15. Representative histograms and TEM images for LEV and SEV are included in Figure 2. Cd9 protein abundance was determined by gel electrophoresis. Total protein was measured with a Qubit Protein Assay Kit and EV suspension was evaporated by vacuum and resuspended in electrophoresis buffer. Three LEV (5µg) and SEV (20µg) samples were loaded into BioRad Mini-Protean TGX Gel 4-20% polyacrylamide gels with Licor Chameleon Duo ladders (928-60000) and run at 20mA for 2 hours. Proteins were transferred to nitrocellulose membrane via 200mA over 3 hours on ice. The membrane was blocked in Licor Intercept Blocking Buffer for 1hour at room temperature then incubated with Cd9 antibody (HI9a Biolegend Cat 312112) at 1:5000 overnight at room temperature. The membrane was then incubated with Licor IRDye

800CW streptavidin (926-32230) at 1:5000 for 2 hours at room temperature and the membrane was imaged by Licor Odyssey.

Flow Cytometry on EVs

EVs surface protein expression was determined by flow cytometry. EVs were resuspended at $1x10^8$/10µL of filtered PBS. Di-8-ANEPPS (Invitrogen Cat# D3167) was reconstituted in ethanol as per manufacturer instruction and further diluted to 1:1000 in filtered PBS. Antibodies were spun at 20,000 x g for 30 minutes at 4°C immediately before use. 10µL of EV suspension was incubated in ANEPPS (10µL) and antibodies, 1.25µL Cd45-Ry586 (Cat# BD568135), 1.25µL Cd41a- PE/Cy7 (Cat# BDB561424), 1.25µL PLAP- eFlour660 (Fisher Cat# 50-112-4573) , and 1.25µL Cd34- PE/CF594 (Cat# BDB562449) and 3µL Cd31-AF700 (Biolegend Cat# 50-207-2950), for 30 minutes at room temperature. 470µL of filtered PBS was added before samples were measured by BD Symphony A1 cytometer. Negative controls included: antibodies alone, EVs without ANEPPS, and EVs treated with 1% triton. Data was analyzed using FlowJo software. EVs were identified by Small Particle Side Scatter (SP-SSC) and expression of ANEPPS.

***In vitro* trophoblast EV co-culture**

BeWo cells, subclone B30, were cultured in 75-cm^2 flasks (Fisher Scientific) at 37°C and 5% CO_2 in media (DMEM/F12, 10% FBS, 1% P/S, 1%L-alanyl-L-glutamine). EV-depleted media was made with EV-depleted FBS (Gibco A2720801) and used for cell culture experiments. Cells were plated at 250,000 cells/well in a 6 well plate and 1.5mL of EV-depleted media was added. Cells adhered for 24 hours before adding 1µg/µL forskolin, cAMP producer, to promote syncytialization for an additional 24 hours. LEVs and SEVs were resuspended in

EV-depleted media at $1x10^6$/mL and added to BeWo cells for an additional 24 hours. At the time of harvest, cell media were collected, and cells released with 0.25% trypsin. Cells were washed and collected as pellets for total DNA measurement and RNA isolation and sequencing. Cell media was spun at 500G to clear cell debris and the supernatant was stored for future hormone measurement. Hormones were measured by Penn Fertility Care using Elecsys HCG+β (Cat# 03271749, Roche Diagnostics) and Elecsys Progesterone III (Cat# 07092539, Roche Diagnostics).

Extravillous trophoblasts (EVTs) were isolated from fresh first trimester placenta based on an EVT outgrowth-based protocol established by Gram et al. (*78-82*). In brief, villous tissue was finely minced and cultured at 37°C and 5% CO_2 in RPMI 1640 media with 20% FBS. After attachment, EVT outgrowth occurs, and those cells were isolated. Isolated EVTs were confirmed by staining for HLA-G and CK7. EVT invasion was measured using the MilliporeSigma Chemicon QCM Collagen Cell Invasion Assay (Cat# ECM558). EVTs were added to the invasion plate with EV-depleted media and large and small EVs at $1x10^6$/mL. Cells were incubated at 37°C and 5% CO_2 for 48 hours. Cells that invaded into the second chamber were quantified using a fluorescent plate reader (SpectraMax).

EV mRNA sequencing

Total RNA was isolated from large and small EVs isolated from 500µL of plasma. Isolated EVs were treated with RNAseA (0.02µg/µL) (Invitrogen Cat# 12091021) for 20 minutes at 37°C to degrade extravesicular RNA. Enzyme activity was stopped by freezing samples at -80°C for 5 minutes and immediate resuspension in Trizol. Nucleic acids were isolated via BCP co-incubation, precipitated by isopropanol, and washed in ethanol. mRNA

libraries were prepared from total RNA using the SMART-Seq protocol (*83*). Briefly, RNA was reverse transcribed using Superscript II (Invitrogen, Cat#18064014). The cDNA was amplified with 20 cycles and cleaned up with AMPure XP beads (Beckman Coulter Cat#A63881). cDNA was quantified with Qubit dsDNA HS Assay Kit (Life Technologies, Inc. Cat#Q32851) and 2ng of each sample was used to construct a pool of uniquely indexed samples (Illumina Cat# FC-131-1096). A second amplification was performed with 12 cycles and cleaned up with AMPure XP beads. The final library was sequenced on a NextSeq 1000. Data were mapped against the hg19 genome using RSEM and normalized to transcripts per million (tpm)(*84*).

While there are differentially expressed transcripts compared to Controls, we chose not to focus on these because the statistical threshold (adjusted p-value <0.05) was rarely met due to high intrasubject variability. Instead, we only considered genes that are uniquely expressed in either Controls or COVID-19 cases. First, we filtered genes to those with greater than 5 transcripts per million and considered these expressed genes. Unique genes were determined to have no expression in any sample of the given group after filtration. Then only genes with expression in the majority (50% or more) of the samples in the comparison group were considered. As an example, a gene is uniquely expressed in R1 compared to Controls if all Controls samples have no expression and 5 or more samples (n=10) in R1 have expression (data in Table 5&6). Unique genes expressed by Controls but not a COVID-19 group are listed in Figure 6. These strict criteria identified genes in each group that are uniquely expressed. Those genes were considered for subsequent analysis.

EV mtDNA measurement

mtDNA was isolated and quantified from large and small EVs by TaqMan-based quantitative polymerase chain reaction (qPCR). We determined $2x10^7$ LEV and $3x10^9$ SEVs

were necessary to reliably and robustly measure mtDNA. The assay quantified mitochondrial-encoded human NADH: ubiquinone oxidoreductase core subunit 1 (ND1) as previously described (*85*). The qPCR reactions were performed in triplicates using a QuantStudio 5 Real-time PCR System (Thermo Fisher) using the following thermocycling conditions: 95 °C for 20 s followed by 40 cycles of 95 °C for 1 s, 63 °C for 20 s, and 60 °C for 20 s. Serial dilutions of pooled human placenta DNA quantified for copies of ND1 (copies/μL) by digital PCR (dPCR) were used as a standard curve. The amount of mtDNA per EV was determined by normalizing the resulting abundance by the number of EVs in starting material. A correlation between the gestational age at infection and the abundance of EV mtDNA was tested.

Statistical Analysis

GraphPad Prism was used to generate graphs and statistically test data. Subject demographics and outcomes were tested by a chi-squared test and considered statistically different if $p<0.05$. Data was tested for normality and either parametric or non-parametric tests were used to determine significance. Data points were identified as outliers and removed if they exceeded two times the standard deviation from the mean. A one-way ANOVA tested for a difference within all groups and subsequent post-hoc t-tests or Kruskal-Wallis determined significance of each COVID-19 group compared to Controls. Pearson's correlation was used to determine a correlation between gestational age at infection and mtDNA abundance. A p-value less than 0.05 was considered significant. Differential gene expression was determined to be significant if the adjusted p-value was less than 0.05 and the fold change greater than 1.5.

List of Supplementary Materials

Supplemental Table 1. Placenta RNAseq DEG

Supplemental Table 2. EV Transcripts Associated with Adverse Pregnancy Outcomes

References and Notes

Acknowledgments: The authors would like to acknowledge the dedication and effort by the Pregnancy and Perinatal Research Center, especially Meaghan McCabe, in enrolling patients and collecting samples. The authors would also like to thank Dr. Jonni Moore and Richard Schretzenmair at the University of Pennsylvania's Cytomics and Shared Resource Laboratory for their guidance in conducting flow cytometry on EVs.

Funding: This research was funded by a COVID-19 grant from the March of Dimes (Parry and Simmons) and two mentored scientist awards from the University of Pennsylvania (Golden, ES019851 – Translational Research Training Program in Environmental Sciences and ES013508 – Mentored Scientist Transition).

Author contributions: Experimental Design: TNG, SM, LA, CCC, RLL, RL, BAK, MM, JFS, SP, and RAS. Data acquisition and analysis: TNG, SM, LA, RLL, CCC, BAK, NAT, and AW. The manuscript was written by TNG, JFS, SP, and RAS and reviewed by all authors.

Competing interests: none

References:

1. A. Conde-Agudelo, R. Romero, SARS-CoV-2 infection during pregnancy and risk of preeclampsia: a systematic review and meta-analysis. *Am J Obstet Gynecol* **226**, 68-89 e63 (2022).
2. S. N. Kazemi *et al.*, COVID-19 and cause of pregnancy loss during the pandemic: A systematic review. *PLoS One* **16**, e0255994 (2021).
3. T. D. Metz *et al.*, Disease Severity and Perinatal Outcomes of Pregnant Patients With Coronavirus Disease 2019 (COVID-19). *Obstet Gynecol* **137**, 571-580 (2021).
4. E. R. Smith *et al.*, Adverse maternal, fetal, and newborn outcomes among pregnant women with SARS-CoV-2 infection: an individual participant data meta-analysis. *BMJ Glob Health* **8**, (2023).
5. T. N. Golden, R. A. Simmons, Maternal and neonatal response to COVID-19. *Am J Physiol Endocrinol Metab* **319**, E315-E319 (2020).
6. R. N. Baergen, D. S. Heller, J. A. Goldstein, Placental Pathology in COVID-19. *Am J Clin Pathol* **154**, 279 (2020).
7. C. M. Corbetta-Rastelli *et al.*, Analysis of placental pathology after COVID-19 by timing and severity of infection. *Am J Obstet Gynecol MFM* **5**, 100981 (2023).
8. F. M. Cribiu *et al.*, Severe SARS-CoV-2 placenta infection can impact neonatal outcome in the absence of vertical transmission. *J Clin Invest* **131**, (2021).
9. B. Joshi *et al.*, The placental pathology in Coronavirus disease 2019 infected mothers and its impact on pregnancy outcome. *Placenta* **127**, 1-7 (2022).
10. E. T. Patberg *et al.*, Coronavirus disease 2019 infection and placental histopathology in women delivering at term. *Am J Obstet Gynecol* **224**, 382 e381-382 e318 (2021).
11. M. C. Sharps *et al.*, A structured review of placental morphology and histopathological lesions associated with SARS-CoV-2 infection. *Placenta* **101**, 13-29 (2020).
12. A. G. Edlow *et al.*, Assessment of Maternal and Neonatal SARS-CoV-2 Viral Load, Transplacental Antibody Transfer, and Placental Pathology in Pregnancies During the COVID-19 Pandemic. *JAMA Netw Open* **3**, e2030455 (2020).
13. J. J. Mulvey, C. M. Magro, L. X. Ma, G. J. Nuovo, R. N. Baergen, Analysis of complement deposition and viral RNA in placentas of COVID-19 patients. *Ann Diagn Pathol* **46**, 151530 (2020).
14. C. Balbi *et al.*, Circulating extracellular vesicles are endowed with enhanced procoagulant activity in SARS-CoV-2 infection. *EBioMedicine* **67**, 103369 (2021).
15. D. Forte *et al.*, Circulating extracellular particles from severe COVID-19 patients show altered profiling and innate lymphoid cell-modulating ability. *Front Immunol* **14**, 1085610 (2023).
16. M. S. George *et al.*, Extracellular vesicles in COVID-19 convalescence can regulate T cell metabolism and function. *iScience* **26**, 107280 (2023).
17. N. Mackman, S. Antoniak, A. S. Wolberg, R. Kasthuri, N. S. Key, Coagulation Abnormalities and Thrombosis in Patients Infected With SARS-CoV-2 and Other Pandemic Viruses. *Arterioscler Thromb Vasc Biol* **40**, 2033-2044 (2020).
18. A. Rosell *et al.*, Patients With COVID-19 Have Elevated Levels of Circulating Extracellular Vesicle Tissue Factor Activity That Is Associated With Severity and Mortality-Brief Report. *Arterioscler Thromb Vasc Biol* **41**, 878-882 (2021).
19. L. Traby *et al.*, Extracellular Vesicles and Citrullinated Histone H3 in Coronavirus Disease 2019 Patients. *Thromb Haemost* **122**, 113-122 (2022).
20. A. Gupta *et al.*, Extrapulmonary manifestations of COVID-19. *Nat Med* **26**, 1017-1032 (2020).
21. F. Puhm, L. Flamand, E. Boilard, Platelet extracellular vesicles in COVID-19: Potential markers and makers. *J Leukoc Biol* **111**, 63-74 (2022).
22. H. K. Siddiqi, P. Libby, P. M. Ridker, COVID-19 - A vascular disease. *Trends Cardiovasc Med* **31**, 1-5 (2021).
23. E. Barberis *et al.*, Circulating Exosomes Are Strongly Involved in SARS-CoV-2 Infection. *Front Mol Biosci* **8**, 632290 (2021).
24. Y. Fujita *et al.*, Early prediction of COVID-19 severity using extracellular vesicle COPB2. *J Extracell Vesicles* **10**, e12092 (2021).
25. K. Mao *et al.*, Proteomics of extracellular vesicles in plasma reveals the characteristics and residual traces of COVID-19 patients without underlying diseases after 3 months of recovery. *Cell Death Dis* **12**, 541 (2021).

26. S. Bhaskar *et al.*, Cytokine Storm in COVID-19-Immunopathological Mechanisms, Clinical Considerations, and Therapeutic Approaches: The REPROGRAM Consortium Position Paper. *Front Immunol* **11**, 1648 (2020).
27. K. H. W. Yim, S. Borgoni, R. Chahwan, Serum extracellular vesicles profiling is associated with COVID-19 progression and immune responses. *J Extracell Biol* **1**, e37 (2022).
28. R. Menon *et al.*, Protein Profile Changes in Circulating Placental Extracellular Vesicles in Term and Preterm Births: A Longitudinal Study. *Endocrinology* **161**, (2020).
29. S. Sarker *et al.*, Placenta-derived exosomes continuously increase in maternal circulation over the first trimester of pregnancy. *J Transl Med* **12**, 204 (2014).
30. C. Salomon *et al.*, A gestational profile of placental exosomes in maternal plasma and their effects on endothelial cell migration. *PLoS One* **9**, e98667 (2014).
31. K. Bai *et al.*, Placenta-Derived Exosomes as a Modulator in Maternal Immune Tolerance During Pregnancy. *Front Immunol* **12**, 671093 (2021).
32. A. G. Lokossou *et al.*, Endogenous retrovirus-encoded Syncytin-2 contributes to exosome-mediated immunosuppression of T cellsdagger. *Biol Reprod* **102**, 185-198 (2020).
33. J. Ratajczak *et al.*, Paracrine proangiopoietic effects of human umbilical cord blood-derived purified CD133+ cells--implications for stem cell therapies in regenerative medicine. *Stem Cells Dev* **22**, 422-430 (2013).
34. M. Arias *et al.*, [Extracellular vesicle concentration in maternal plasma as an early marker of gestational diabetes]. *Rev Med Chil* **147**, 1503-1509 (2019).
35. X. Chang *et al.*, Exosomes From Women With Preeclampsia Induced Vascular Dysfunction by Delivering sFlt (Soluble Fms-Like Tyrosine Kinase)-1 and sEng (Soluble Endoglin) to Endothelial Cells. *Hypertension* **72**, 1381-1390 (2018).
36. R. Gadde, D. Cd, S. R. Sheela, Placental protein 13: An important biological protein in preeclampsia. *J Circ Biomark* **7**, 1849454418786159 (2018).
37. I. Hromadnikova, L. Dvorakova, K. Kotlabova, L. Krofta, The Prediction of Gestational Hypertension, Preeclampsia and Fetal Growth Restriction via the First Trimester Screening of Plasma Exosomal C19MC microRNAs. *Int J Mol Sci* **20**, (2019).
38. P. Pillay, N. Maharaj, J. Moodley, I. Mackraj, Placental exosomes and pre-eclampsia: Maternal circulating levels in normal pregnancies and, early and late onset pre-eclamptic pregnancies. *Placenta* **46**, 18-25 (2016).
39. P. Pillay, K. Moodley, J. Moodley, I. Mackraj, Placenta-derived exosomes: potential biomarkers of preeclampsia. *Int J Nanomedicine* **12**, 8009-8023 (2017).
40. P. Pillay, M. Vatish, R. Duarte, J. Moodley, I. Mackraj, Exosomal microRNA profiling in early and late onset preeclamptic pregnant women reflects pathophysiology. *Int J Nanomedicine* **14**, 5637-5657 (2019).
41. C. Salomon *et al.*, Gestational Diabetes Mellitus Is Associated With Changes in the Concentration and Bioactivity of Placenta-Derived Exosomes in Maternal Circulation Across Gestation. *Diabetes* **65**, 598-609 (2016).
42. M. V. C. Barnes, P. Pantazi, B. Holder, Circulating extracellular vesicles in healthy and pathological pregnancies: A scoping review of methodology, rigour and results. *J Extracell Vesicles* **12**, e12377 (2023).
43. O. Parant *et al.*, CD34+ cells in maternal placental blood are mainly fetal in origin and express endothelial markers. *Lab Invest* **89**, 915-923 (2009).
44. C. Salomon *et al.*, Hypoxia-induced changes in the bioactivity of cytotrophoblast-derived exosomes. *PLoS One* **8**, e79636 (2013).
45. P. Kaufmann, S. Black, B. Huppertz, Endovascular trophoblast invasion: implications for the pathogenesis of intrauterine growth retardation and preeclampsia. *Biol Reprod* **69**, 1-7 (2003).
46. P. Tantbirojn, C. P. Crum, M. M. Parast, Pathophysiology of placenta creta: the role of decidua and extravillous trophoblast. *Placenta* **29**, 639-645 (2008).
47. Y. S. Chan, L. Yang, H. H. Ng, Transcriptional regulatory networks in embryonic stem cells. *Prog Drug Res* **67**, 239-252 (2011).
48. M. Prieto-Vila, Y. Yoshioka, T. Ochiya, Biological Functions Driven by mRNAs Carried by Extracellular Vesicles in Cancer. *Front Cell Dev Biol* **9**, 620498 (2021).
49. M. C. Deregibus *et al.*, Endothelial progenitor cell derived microvesicles activate an angiogenic program in endothelial cells by a horizontal transfer of mRNA. *Blood* **110**, 2440-2448 (2007).
50. J. Guduric-Fuchs *et al.*, Selective extracellular vesicle-mediated export of an overlapping set of microRNAs from multiple cell types. *BMC Genomics* **13**, 357 (2012).

51. P. Jenjaroenpun *et al.*, Characterization of RNA in exosomes secreted by human breast cancer cell lines using next-generation sequencing. *PeerJ* **1**, e201 (2013).
52. K. M. Kim, K. Abdelmohsen, M. Mustapic, D. Kapogiannis, M. Gorospe, RNA in extracellular vesicles. *Wiley Interdiscip Rev RNA* **8**, (2017).
53. E. N. Nolte-'t Hoen *et al.*, Deep sequencing of RNA from immune cell-derived vesicles uncovers the selective incorporation of small non-coding RNA biotypes with potential regulatory functions. *Nucleic Acids Res* **40**, 9272-9285 (2012).
54. J. Ratajczak *et al.*, Embryonic stem cell-derived microvesicles reprogram hematopoietic progenitors: evidence for horizontal transfer of mRNA and protein delivery. *Leukemia* **20**, 847-856 (2006).
55. J. Skog *et al.*, Glioblastoma microvesicles transport RNA and proteins that promote tumour growth and provide diagnostic biomarkers. *Nat Cell Biol* **10**, 1470-1476 (2008).
56. H. Valadi *et al.*, Exosome-mediated transfer of mRNAs and microRNAs is a novel mechanism of genetic exchange between cells. *Nat Cell Biol* **9**, 654-659 (2007).
57. Z. Wei *et al.*, Coding and noncoding landscape of extracellular RNA released by human glioma stem cells. *Nat Commun* **8**, 1145 (2017).
58. M. Peris, K. Crompton, D. A. Shepherd, D. J. Amor, The association between human chorionic gonadotropin and adverse pregnancy outcomes: a systematic review and meta-analysis. *Am J Obstet Gynecol* **230**, 118-184 (2024).
59. J. D. Domizio *et al.*, The cGAS-STING pathway drives type I IFN immunopathology in COVID-19. *Nature* **603**, 145-151 (2022).
60. M. I. Faizan *et al.*, NSP4 and ORF9b of SARS-CoV-2 Induce Pro-Inflammatory Mitochondrial DNA Release in Inner Membrane-Derived Vesicles. *Cells* **11**, (2022).
61. L. Gibellini *et al.*, Altered bioenergetics and mitochondrial dysfunction of monocytes in patients with COVID-19 pneumonia. *EMBO Mol Med* **12**, e13001 (2020).
62. Y. Mo *et al.*, Mitochondrial Dysfunction Associates With Acute T Lymphocytopenia and Impaired Functionality in COVID-19 Patients. *Front Immunol* **12**, 799896 (2021).
63. M. Tian *et al.*, HIF-1alpha promotes SARS-CoV-2 infection and aggravates inflammatory responses to COVID-19. *Signal Transduct Target Ther* **6**, 308 (2021).
64. B. Appelman *et al.*, Muscle abnormalities worsen after post-exertional malaise in long COVID. *Nat Commun* **15**, 17 (2024).
65. D. Scozzi *et al.*, Circulating mitochondrial DNA is an early indicator of severe illness and mortality from COVID-19. *JCI Insight* **6**, (2021).
66. S. Shoraka, S. R. Mohebbi, S. M. Hosseini, M. R. Zali, Comparison of plasma mitochondrial DNA copy number in asymptomatic and symptomatic COVID-19 patients. *Front Microbiol* **14**, 1256042 (2023).
67. J. J. Valdes-Aguayo *et al.*, Peripheral Blood Mitochondrial DNA Levels Were Modulated by SARS-CoV-2 Infection Severity and Its Lessening Was Associated With Mortality Among Hospitalized Patients With COVID-19. *Front Cell Infect Microbiol* **11**, 754708 (2021).
68. T. J. Costa *et al.*, Mitochondrial DNA and TLR9 activation contribute to SARS-CoV-2-induced endothelial cell damage. *Vascul Pharmacol* **142**, 106946 (2022).
69. L. Peruzzotti-Jametti *et al.*, Neural stem cells traffic functional mitochondria via extracellular vesicles. *PLoS Biol* **19**, e3001166 (2021).
70. D. G. Phinney *et al.*, Mesenchymal stem cells use extracellular vesicles to outsource mitophagy and shuttle microRNAs. *Nat Commun* **6**, 8472 (2015).
71. P. Sansone *et al.*, Packaging and transfer of mitochondrial DNA via exosomes regulate escape from dormancy in hormonal therapy-resistant breast cancer. *Proc Natl Acad Sci U S A* **114**, E9066-E9075 (2017).
72. M. Schorpp-Kistner, Z. Q. Wang, P. Angel, E. F. Wagner, JunB is essential for mammalian placentation. *EMBO J* **18**, 934-948 (1999).
73. A. M. Nuzzo *et al.*, JunB/cyclin-D1 imbalance in placental mesenchymal stromal cells derived from preeclamptic pregnancies with fetal-placental compromise. *Placenta* **35**, 483-490 (2014).
74. A. T. Papageorghiou *et al.*, Preeclampsia and COVID-19: results from the INTERCOVID prospective longitudinal study. *Am J Obstet Gynecol* **225**, 289 e281-289 e217 (2021).
75. A. A. Freedman, L. S. Keenan-Devlin, A. Borders, G. E. Miller, L. M. Ernst, Formulating a Meaningful and Comprehensive Placental Phenotypic Classification. *Pediatr Dev Pathol* **24**, 337-350 (2021).
76. T. Y. Khong *et al.*, Sampling and Definitions of Placental Lesions: Amsterdam Placental Workshop Group Consensus Statement. *Arch Pathol Lab Med* **140**, 698-713 (2016).

77. R. W. Redline, S. Ravishankar, C. M. Bagby, S. T. Saab, S. Zarei, Four major patterns of placental injury: a stepwise guide for understanding and implementing the 2016 Amsterdam consensus. *Mod Pathol* **34**, 1074-1092 (2021).
78. L. Anton, A. G. Brown, S. Parry, M. A. Elovitz, Lipopolysaccharide induces cytokine production and decreases extravillous trophoblast invasion through a mitogen-activated protein kinase-mediated pathway: possible mechanisms of first trimester placental dysfunction. *Hum Reprod* **27**, 61-72 (2012).
79. L. Anton *et al.*, HIF-1alpha Stabilization Increases miR-210 Eliciting First Trimester Extravillous Trophoblast Mitochondrial Dysfunction. *Front Physiol* **10**, 699 (2019).
80. S. Getsios, G. T. Chen, D. T. Huang, C. D. MacCalman, Regulated expression of cadherin-11 in human extravillous cytotrophoblasts undergoing aggregation and fusion in response to transforming growth factor beta 1. *J Reprod Fertil* **114**, 357-363 (1998).
81. C. H. Graham, J. J. Lysiak, K. R. McCrae, P. K. Lala, Localization of transforming growth factor-beta at the human fetal-maternal interface: role in trophoblast growth and differentiation. *Biol Reprod* **46**, 561-572 (1992).
82. J. Y. Park *et al.*, A microphysiological model of human trophoblast invasion during implantation. *Nat Commun* **13**, 1252 (2022).
83. J. J. Trombetta *et al.*, Preparation of Single-Cell RNA-Seq Libraries for Next Generation Sequencing. *Curr Protoc Mol Biol* **107**, 4 22 21-24 22 17 (2014).
84. O. Yukselen, O. Turkyilmaz, A. R. Ozturk, M. Garber, A. Kucukural, DolphinNext: a distributed data processing platform for high throughput genomics. *BMC Genomics* **21**, 310 (2020).
85. S. A. Ware *et al.*, An automated, high-throughput methodology optimized for quantitative cell-free mitochondrial and nuclear DNA isolation from plasma. *J Biol Chem* **295**, 15677-15691 (2020).
86. K. S. Rehman, S. Yin, B. A. Mayhew, R. A. Word, W. E. Rainey, Human myometrial adaptation to pregnancy: cDNA microarray gene expression profiling of myometrium from non-pregnant and pregnant women. *Mol Hum Reprod* **9**, 681-700 (2003).
87. C. M. Whittington *et al.*, Transcriptomic changes in the pre-implantation uterus highlight histotrophic nutrition of the developing marsupial embryo. *Sci Rep* **8**, 2412 (2018).
88. S. Peng *et al.*, Genetic regulation of the placental transcriptome underlies birth weight and risk of childhood obesity. *PLoS Genet* **14**, e1007799 (2018).
89. J. L. Maron *et al.*, Gene expression analysis in pregnant women and their infants identifies unique fetal biomarkers that circulate in maternal blood. *J Clin Invest* **117**, 3007-3019 (2007).
90. G. Song, F. W. Bazer, T. E. Spencer, Differential expression of cathepsins and cystatin C in ovine uteroplacental tissues. *Placenta* **28**, 1091-1098 (2007).
91. C. P. Chen *et al.*, Altered placental syncytin and its receptor ASCT2 expression in placental development and pre-eclampsia. *BJOG* **113**, 152-158 (2006).
92. K. L. Fulghum *et al.*, Metabolic signatures of pregnancy-induced cardiac growth. *Am J Physiol Heart Circ Physiol* **323**, H146-H164 (2022).
93. M. Prater *et al.*, RNA-Seq reveals changes in human placental metabolism, transport and endocrinology across the first-second trimester transition. *Biol Open* **10**, (2021).
94. M. B. Rabaglino, J. M. Sanchez, M. McDonald, E. O'Callaghan, P. Lonergan, Maternal blood transcriptome as a sensor of foetal organ maturation at the end of organogenesis in cattle. *Biol Reprod*, (2023).
95. C. Y. Hung *et al.*, A defect in the inner kinetochore protein CENPT causes a new syndrome of severe growth failure. *PLoS One* **12**, e0189324 (2017).
96. W. Li *et al.*, Role of IGF2BP3 in trophoblast cell invasion and migration. *Cell Death Dis* **5**, e1025 (2014).
97. H. Wen, L. Chen, J. He, J. Lin, MicroRNA expression profiles and networks in placentas complicated with selective intrauterine growth restriction. *Mol Med Rep* **16**, 6650-6673 (2017).
98. G. Wang *et al.*, Impact of intrauterine exposure to maternal diabetes on preterm birth: fetal DNA methylation alteration is an important mediator. *Clin Epigenetics* **15**, 59 (2023).
99. I. L. Aye, T. L. Powell, T. Jansson, Review: Adiponectin--the missing link between maternal adiposity, placental transport and fetal growth? *Placenta* **34 Suppl**, S40-45 (2013).
100. I. Hromadnikova *et al.*, Expression profile of C19MC microRNAs in placental tissue in pregnancy-related complications. *DNA Cell Biol* **34**, 437-457 (2015).
101. Y. Gu, S. A. Burlison, Y. Wang, PAF levels and PAF-AH activities in placentas from normal and preeclamptic pregnancies. *Placenta* **27**, 744-749 (2006).

102. T. Garrido-Gomez *et al.*, Severe pre-eclampsia is associated with alterations in cytotrophoblasts of the smooth chorion. *Development* **144**, 767-777 (2017).
103. R. Calicchio *et al.*, Preeclamptic plasma induces transcription modifications involving the AP-1 transcriptional regulator JDP2 in endothelial cells. *Am J Pathol* **183**, 1993-2006 (2013).
104. W. Fan *et al.*, Upregulation of METTL14 contributes to trophoblast dysfunction by elevating FOXO3a expression in an m(6)A-dependent manner. *Placenta* **124**, 18-27 (2022).
105. J. Wang, F. Gao, X. Zhao, Y. Cai, H. Jin, Integrated analysis of the transcriptome-wide m6A methylome in preeclampsia and healthy control placentas. *PeerJ* **8**, e9880 (2020).
106. M. Diaz *et al.*, Placental and Cord Blood Methylation of Genes Involved in Energy Homeostasis: Association With Fetal Growth and Neonatal Body Composition. *Diabetes* **66**, 779-784 (2017).
107. P. Murthi, G. Rajaraman, J. Erwich, E. Dimitriadis, Decreased Placental FPR2 in Early Pregnancies That Later Developed Small-For-Gestation Age: A Potential Role of FPR2 in the Regulation of Epithelial-Mesenchymal Transition. *Cells* **9**, (2020).
108. A. Chu *et al.*, Aldehyde dehydrogenase isoforms and inflammatory cell populations are differentially expressed in term human placentas affected by intrauterine growth restriction. *Placenta* **81**, 9-17 (2019).
109. A. Dobierzewska *et al.*, Impairment of Angiogenic Sphingosine Kinase-1/Sphingosine-1-Phosphate Receptors Pathway in Preeclampsia. *PLoS One* **11**, e0157221 (2016).
110. M. H. Fenstad *et al.*, Genetic and molecular functional characterization of variants within TNFSF13B, a positional candidate preeclampsia susceptibility gene on 13q. *PLoS One* **5**, (2010).
111. J. G. Grudzinskas *et al.*, Identification of high-risk pregnancy by the routine measurement of pregnancy-specific beta 1-glycoprotein. *Am J Obstet Gynecol* **147**, 10-12 (1983).
112. K. Pihl, T. Larsen, I. Laursen, L. Krebs, M. Christiansen, First trimester maternal serum pregnancy-specific beta-1-glycoprotein (SP1) as a marker of adverse pregnancy outcome. *Prenat Diagn* **29**, 1256-1261 (2009).
113. R. M. Silver, K. D. Heyborne, K. K. Leslie, Pregnancy specific beta 1 glycoprotein (SP-1) in maternal serum and amniotic fluid; pre-eclampsia, small for gestational age fetus and fetal distress. *Placenta* **14**, 583-589 (1993).
114. M. A. Mohamad *et al.*, A Review of Candidate Genes and Pathways in Preeclampsia-An Integrated Bioinformatical Analysis. *Biology (Basel)* **9**, (2020).
115. B. Vora *et al.*, Meta-Analysis of Maternal and Fetal Transcriptomic Data Elucidates the Role of Adaptive and Innate Immunity in Preterm Birth. *Front Immunol* **9**, 993 (2018).
116. M. N. Moufarrej *et al.*, Early prediction of preeclampsia in pregnancy with cell-free RNA. *Nature* **602**, 689-694 (2022).
117. J. Shang, L. Lin, X. Huang, L. Zhou, Q. Huang, Re-expression of circ_0043610 contributes to trophoblast dysfunction through the miR-558/RYBP pathway in preeclampsia. *Endocr J* **69**, 1373-1385 (2022).
118. C. Shu, P. Xu, J. Han, S. Han, J. He, Upregulation of circRNA hsa_circ_0008726 in Pre-eclampsia Inhibits Trophoblast Migration, Invasion, and EMT by Regulating miR-345-3p/RYBP Axis. *Reprod Sci* **29**, 2829-2841 (2022).
119. Y. Zhang, S. Fang, J. Wang, S. Chen, R. Xuan, Hsa_circ_0008726 regulates the proliferation, migration, and invasion of trophoblast cells in preeclampsia through modulating the miR-1290-LHX6 signaling pathway. *J Clin Lab Anal* **36**, e24540 (2022).
120. J. Wang *et al.*, Alpha-2-macroglobulin is involved in the occurrence of early-onset pre-eclampsia via its negative impact on uterine spiral artery remodeling and placental angiogenesis. *BMC Med* **21**, 90 (2023).
121. J. A. Tronco *et al.*, Alpha-2-macroglobulin from circulating exosome-like vesicles is increased in women with preterm pregnancies. *Sci Rep* **10**, 16961 (2020).
122. K. Leavey, S. L. Wilson, S. A. Bainbridge, W. P. Robinson, B. J. Cox, Epigenetic regulation of placental gene expression in transcriptional subtypes of preeclampsia. *Clin Epigenetics* **10**, 28 (2018).
123. R. K. Yuen, M. S. Penaherrera, P. von Dadelszen, D. E. McFadden, W. P. Robinson, DNA methylation profiling of human placentas reveals promoter hypomethylation of multiple genes in early-onset preeclampsia. *Eur J Hum Genet* **18**, 1006-1012 (2010).
124. J. Pan, X. Tian, H. Huang, N. Zhong, Proteomic Study of Fetal Membrane: Inflammation-Triggered Proteolysis of Extracellular Matrix May Present a Pathogenic Pathway for Spontaneous Preterm Birth. *Front Physiol* **11**, 800 (2020).
125. T. Lekva *et al.*, Dysregulated non-coding telomerase RNA component and associated exonuclease XRN1 in leucocytes from women developing preeclampsia-possible link to enhanced senescence. *Sci Rep* **11**, 19735 (2021).

126. W. Lai, L. Yu, Elevated MicroRNA 183 Impairs Trophoblast Migration and Invasiveness by Downregulating FOXP1 Expression and Elevating GNG7 Expression during Preeclampsia. *Mol Cell Biol* **41**, (2020).
127. J. Chen *et al.*, Silencing of long non-coding RNA NEAT1 improves Treg/Th17 imbalance in preeclampsia via the miR-485-5p/AIM2 axis. *Bioengineered* **12**, 8768-8777 (2021).
128. S. Gremlich *et al.*, The long non-coding RNA NEAT1 is increased in IUGR placentas, leading to potential new hypotheses of IUGR origin/development. *Placenta* **35**, 44-49 (2014).
129. J. Schuster *et al.*, Protein Network Analysis of Whole Exome Sequencing of Severe Preeclampsia. *Front Genet* **12**, 765985 (2021).
130. Z. Miao, M. Chen, H. Wu, H. Ding, Z. Shi, Comparative proteomic profile of the human placenta in normal and fetal growth restriction subjects. *Cell Physiol Biochem* **34**, 1701-1710 (2014).
131. J. Zhao *et al.*, The m(6)A methyltransferase METTL3 promotes trophoblast cell invasion by regulating MYLK expression. *Placenta* **129**, 1-6 (2022).
132. J. Zadora *et al.*, Disturbed Placental Imprinting in Preeclampsia Leads to Altered Expression of DLX5, a Human-Specific Early Trophoblast Marker. *Circulation* **136**, 1824-1839 (2017).
133. H. Tiensuu *et al.*, Human placental proteomics and exon variant studies link AAT/SERPINA1 with spontaneous preterm birth. *BMC Med* **20**, 141 (2022).
134. F. Zhou, T. Cheng, Y. Xing, H. Ma, L. Yang, Network exploration of gene signatures underlying low birth weight induced metabolic alterations. *Medicine (Baltimore)* **101**, e31489 (2022).
135. M. A. Deyssenroth *et al.*, Whole-transcriptome analysis delineates the human placenta gene network and its associations with fetal growth. *BMC Genomics* **18**, 520 (2017).
136. D. A. Enquobahrie, C. Qiu, S. Y. Muhie, M. A. Williams, Maternal peripheral blood gene expression in early pregnancy and preeclampsia. *Int J Mol Epidemiol Genet* **2**, 78-94 (2011).
137. A. K. Edwards, K. A. Dunlap, T. E. Spencer, M. C. Satterfield, Identification of Pathways Associated with Placental Adaptation to Maternal Nutrient Restriction in Sheep. *Genes (Basel)* **11**, (2020).

Demographics	Controls (n=32)	R1 (n=15)	R2 (n=20)	R3 (n=22)	AI (n=21)
Maternal age (years)	21 – 42 (Mean: 31.8)	25 - 43 (Mean: 31.7)	18 – 39 (Mean: 29.4)	21 – 42 (Mean: 30.5)	20 – 40 (Mean: 29.4)
Race: White	50%	46.7%	34%	27.3%	9.5%*
Race: Black	41%	46.7%	55%	68.2%*	76.2%*
Race: Asian	9.4%	0%	10%	0%	9.5%
Race: Other/Unknown	0%	6.7%	0%	4.5%	4.8%
GA at delivery (weeks)	37.3 – 41.1 (Mean: 39.3)	35.1 – 40.3 (Mean: 39.1)	33.7 – 41.3 (Mean: 38.4)	32.3 – 39.7 (Mean: 37.5)*	31 – 41 (Mean: 38.1)*
COVID severity	Controls (n=32)	R1 (n=15)	R2 (n=20)	R3 (n=22)	AI (n=21)
Symptomatic	N/A	73.3%	85%	81.8%	14.3%
Asymptomatic	N/A	26.7%	15%	18.2%	85.7%$^{+}$
Hospitalized	N/A	13.3%	0%	31.8%	4.8%
Pregnancy outcomes	Controls (n=32)	R1 (n=15)	R2 (n=20)	R3 (n=22)	AI (n=21)
GHTN	18.8%	53.3%*$^{+}$	20%	13.6%	9.5%
CHTN	3.1%	0%	5%	13.6%	4.8%
Preeclampsia	0%	0%	5%	18.2%*	19%*
Spontaneous PTB	0%	0%	20%*	4.5%	4.8%
Medically indicated PTB	0%	6.7%	10%	18.2%*	19%*
IUGR	6.3%	13.3%	0%	9.1%	4.8%
IUFD	0%	0%	0%	4.5%	0%
Placenta Pathology	Control (n=26)	R1 (n=9)	R2 (n=17)	R3 (n=19)	AI (n=19)
MVM or FVM	26.9%	100%*	71%*	63%*	82.6%*
MVM	15%	44%*	47%*	37%	53%*
High grade MVM	0%	11%	18%*	16%*	11%
FVM	15%	78%*	59%*	42%*	47%*
>10% perivillous fibrin deposition	0%	11%	18%*	21%*	5%

Table 1. Subject demographics, pregnancy outcomes, and placenta pathology
Subjects enrolled in the COMET study formed five groups (controls, resolved infection in the 1st trimester (R1), 2nd trimester (R2), and 3rd trimester (R3), and active infection (AI). Maternal demographics including maternal age, race, and gestational age (GA) at birth are reported. The severity of COVID-19 during their pregnancy, incidence of pregnancy complications (gestational hypertension (gHTN), chronic hypertension (cHTN), preeclampsia, spontaneous and medically indicated preterm birth (PTB), intrauterine growth restriction (IUGR), and intrauterine demise (IUFD)) and placental pathology (maternal vascular malperfusion (MVM), fetal vascular malperfusion (FVM) and perivillous fibrin deposition) are reported * $p<0.05$ chi-squared test compared to Controls.

Control v. R1 Placenta Transcriptome				
canonical pathway	**FC**	**Z-score**	**p-value**	**# genes**
Tumor Microenvironment Pathway	4.61	1	0.00	4
Osteoarthritis Pathway	2.83	nc	0.00	3
Hematopoiesis from Multipotent Stem Cells	1.94	nc	0.01	1
IL-17 Signaling	1.86	nc	0.01	2
Granulocyte Adhesion and Diapedesis	1.85	nc	0.01	2
Hepatic Fibrosis / Hepatic Stellate Cell Activation	1.83	nc	0.01	2
Differential Regulation of Cytokine Production in Macrophages and T Helper Cells by IL-17A and IL-17F	1.76	nc	0.02	1
Agranulocyte Adhesion and Diapedesis	1.75	nc	0.02	2
Pyrimidine Deoxyribonucleotides De Novo Biosynthesis I	1.66	nc	0.02	1
Differential Regulation of Cytokine Production in Intestinal Epithelial Cells by IL-17A and IL-17F	1.66	nc	0.02	1
Control v. R3 Placenta Transcriptome				
canonical pathway	**FC**	**Z-score**	**p-value**	**# genes**
Hepatic Fibrosis / Hepatic Stellate Cell Activation	2.95	nc	0.00	4
Tumor Microenvironment Pathway	2.07	nc	0.01	3
ILK Signaling	1.93	nc	0.01	3
RAR Activation	1.91	nc	0.01	3
RHOGDI Signaling	1.85	nc	0.01	3
Autophagy	1.85	nc	0.01	3
VDR/RXR Activation	1.84	nc	0.01	2
Estrogen Receptor Signaling	1.81	-1	0.02	4
TR/RXR Activation	1.78	nc	0.02	2
AMPK Signaling	1.71	nc	0.02	3
Control v. AI Placenta Transcriptome				
canonical pathway	**FC**	**Z-score**	**p-value**	**# genes**
Phagosome Formation	16.90	-5.44	1.26E-17	17
CREB Signaling in Neurons	11.50	-3.78	3.16E-12	26
Hepatic Fibrosis / Hepatic Stellate Cell Activation	11.00	nc	1.00E-11	26
GP6 Signaling Pathway	11.00	-3.00	1.00E-11	37
Atherosclerosis Signaling	10.80	nc	1.58E-11	41
G-Protein Coupled Receptor Signaling	9.46	-3.79	3.47E-10	19
Breast Cancer Regulation by Stathmin1	8.88	-4.23	1.32E-09	19
Pulmonary Fibrosis Idiopathic Signaling Pathway	8.56	-2.60	2.75E-09	23
Role of Macrophages, Fibroblasts and Endothelial Cells in Rheumatoid Arthritis	8.50	nc	3.16E-09	42
Tumor Microenvironment Pathway	6.88	-2.00	1.32E-07	54

Table 2. Placenta RNAseq canonical pathways
Ingenuity pathway analysis was used to identify altered pathways in placenta collected from COVID-19 groups compared to control. The top 10 altered pathways are listed for each comparison and the log 2-fold change (FC), z-score, p-value, and number of pathway associated genes are reported. In the event a Z-score is not calculated, nc is reported.

BeWo Transcriptome Following Exposure to Control v. AI EVs			
gene symbol	**gene name**	**FC**	**adj p-value**
RNU6-942P	RNA, U6 Small Nuclear 942, Pseudogene	4.41	1.88E-02
RN7SKP203	RN7SK Pseudogene 203	2.12	4.11E-03
FP236383.2	unknown	1.93	7.35E-07
AC068987.3	unknown	1.77	1.46E-02
HIST1H2AE	H2A clustered histone 8	1.74	2.97E-04
AC092127.2	unknown	1.73	1.69E-04
HIST2H2BF	H2B clustered histone 18	1.70	2.97E-04
HIST1H2BO	H2B clustered histone 17	1.68	3.33E-06
HIST1H2BN	H2B clustered histone 15	1.65	3.01E-21
HIST1H2AL	H2A clustered histone 16	1.62	1.18E-02

Table 3. BeWo RNAseq DEG
Transcriptomics of BeWo cells following exposure to EVs identified differentially expressed genes when comparing exposure to AI vs. Controls EVs. The top 10 DEGs are listed for each comparison including the log 2-fold change (FC) and adjusted p-value for each comparison.

BeWo Transcriptome Following Exposure to Control v. AI EVs			
canonical pathway	**FC**	**p-value**	**# genes**
NAD Signaling Pathway	4.99	0.00	4
Granzyme A Signaling	3.86	0.00	2
DNA Methylation and Transcriptional Repression Signaling	3.19	0.00	2
Transcriptional Regulatory Network in Embryonic Stem Cells	2.95	0.00	2
NER (Nucleotide Excision Repair, Enhanced Pathway)	2.39	0.00	2
Ferroptosis Signaling Pathway	2.19	0.01	2
Sirtuin Signaling Pathway	1.53	0.03	2
nNOS Signaling in Neurons	1.37	0.04	1

Table 4. BeWo RNAseq pathway
Ingenuity pathway analysis identified canonical pathways altered following AI EV exposure compared to Controls EV exposure. The top 10 pathways are listed with the log 2-fold change (FC), p-value and number of pathway associated genes.

Uniquely Expressed Transcripts in COVID LEVs					
Gene Symbol	**Gene Name**	**Group(s) with Unique Expression**	**Cellular Function**	**High Trophoblast Expression**	**Increased in Pregnancy**
YY1AP1	YY1 Associated Protein 1	R1, R2	Transcription		
MOSPD1	Motile Sperm Domain Containing 1	R1, AI	Transcription		
RYBP	RING1 And YY1 Binding Protein	R1, AI	Transcription	Y	
H1-4	H1.4 linker histone, cluster member	R2, R3	Unknown		
A2M	Alpha-2-Macroglobulin	R1	Immune		
KIFAP3	Kinesin Associated Protein 3	R1	Chromosome Movement		Y(*86*)
MXD1	MAX Dimerization Protein 1	R1	Proliferation		
PEX19	Peroxisomal Biogenesis Factor 19	R1	Oxidative stress	Y	
TOB1	Transducer Of ERBB2, 1	R1	Proliferation		
HK1	Hexokinase 1	R2	Metabolism	Y	
LY9	Lymphocyte Antigen 9	R2	Immune		Y(*87*)
POLR3C	RNA Polymerase III Subunit C	R2	Nucleic acid binding activity		
SPNS3	SPNS Lysolipid Transporter 3, Sphingosine-1-Phosphate (Putative)	R2	Transporter Activity		
WDR46	WD Repeat Domain 46	R2	Nucleic acid binding activity		
CDC34	Cell Division Cycle 34, Ubiquitin Conjugating Enzyme	R3	Ubiquitination		
FUNDC2	FUN14 Domain Containing 2	R3	Metabolism		
LINC-PINT	Long Intergenic Non-Protein Coding RNA, P53 Induced Transcript	R3	Unknown		
R3HCC1	R3H Domain and Coiled-Coil Containing 1	R3	Nucleic acid binding activity		
ATPSCKMT	ATP Synthase C Subunit Lysine N-Methyltransferase	AI	Mitochondrial ATP synthesis		
DTWD1	DTW Domain Containing 1	AI	Translation		
FBXL4	F-Box and Leucine Rich Repeat Protein 4	AI	Ubiquitination		
FRA10AC1	FRA10A Associated CGG Repeat 1	AI	Transcription		
FOXP1	Forkhead Box P1	AI	Transcription		
GOLGA4	Golgi A4	AI	Protein and lipid transport	Y	Y(*86*)
GPBP1L1	GC-Rich Promoter Binding Protein 1 Like 1	AI	Transcription		
IL1R2	Interleukin 1 Receptor Type 2	AI	Immune		

KIAA1143	KIAA1143	AI	Unknown		
LINC01410	Long Intergenic Non-Protein Coding RNA 1410	AI	Unknown		
NEAT1	Nuclear Paraspeckle Assembly Transcript 1	AI	Transcription	Y	
WDR26	WD Repeat Domain 26	AI	Cell cycle progression and gene regulation	Y	
XRN1	5'-3' Exoribonuclease 1	AI	mRNA degradation		Y(*88*)
ZNF638	Zinc Finger Protein 638	AI	Transcription		

Table 5. Unique genes identified in LEVs isolated from COVID-19 cases
Transcripts are carried by LEVs isolated from COVID-19 cases that are absent in Controls. The listed transcripts are not detected in LEVs isolated from Controls but are present in most samples in the identified COVID-19 groups. The cellular function, expression in trophoblasts, and pregnancy associated expression of each transcript is listed as well (reference listed).

Uniquely Expressed Transcripts in COVID SEVs					
Gene Symbol	**Gene Name**	**Group with Unique Expression**	**Cellular Function**	**High Trophoblast Expression**	**Increased in Pregnancy**
MYL4	Myosin Light Chain 4	R1, AI	Motor Protein		Y(*89*)
C18orf32	Chromosome 18 Open Reading Frame 32	R1, AI	Immune	Y	
CAPG	Capping Actin Protein, Gelsolin Like	R2, AI	Motor Protein		
CTSS	Cathepsin S	R3, AI	Immune		Y(*90*)
CYREN	Cell Cycle Regulator Of NHEJ	R1	DNA Repair		
CCDC124	Coiled-Coil Domain Containing 124	R1	Transcription		
CD27-AS1	CD27 Antisense RNA 1	R1	Immune		
GNB2	G Protein Subunit Beta 2	R1	G Protein Signaling		
PHF5A	PHD Finger Protein 5A	R1	Immune	Y	
RBM8A	RNA Binding Motif Protein 8A	R1	Transcription	Y	
SIGMAR1	Sigma Non-Opioid Intracellular Receptor 1	R1	Calcium Signaling	Y	
CSF3R	Colony Stimulating Factor 3 Receptor	R2	Immune	Y	
ESD	Esterase D	R2	Metabolism		
GTF2IRD2	GTF2I Repeat Domain Containing 2	R2	Transcription		
SLC1A5	Solute Carrier Family 1 Member 5	R2	Metabolism	Y	Y(*91*)
AUP1	AUP1 Lipid Droplet Regulating VLDL Assembly Factor	R3	Ubiquitination	Y	
MFF	Mitochondrial Fission Factor	R3	Mitochondrial and Peroxisomal Fission		
ARCN1	Archain 1	AI	Vesicle	Y	
CKAP2	Cytoskeleton Associated Protein 2	AI	Proliferation		Y(*92*)
CSNK2B	Casein Kinase 2 Beta	AI	Metabolism		
CYP27C1	Cytochrome P450 Family 27 Subfamily C Member 1	AI	Metabolism		
GRHL1	Grainyhead Like Transcription Factor 1	AI	Epithelial Development	Y	
HSP90B1	Heat Shock Protein 90 Beta Family Member 1	AI	Molecular Chaperone	Y	Y(*93*)
KIF5B	Kinesin Family Member 5B	AI	Protein Binding Activity		
LINC01123	Long Intergenic Non-Protein Coding RNA 1123	AI	Unknown		
LOC728323	unknown	AI	Unknown		
MANBAL	Mannosidase Beta Like	AI	Membrane Protein		Y(*94*)

MUC22	Mucin 22	AI	Membrane Protein		
MYLK	Myosin Light Chain Kinase	AI	Contractile Activity		
OR4F17	Olfactory Receptor Family 4 Subfamily F Member 17	AI	Vesicle		
PARP9	Poly (ADP-Ribose) Polymerase Family Member 9	AI	Immune		
RNF2	Ring Finger Protein 2	AI	Transcription		
SAR1A	Secretion Associated Ras Related GTPase 1A	AI	Vesicle	Y	
SHC4	SHC Adaptor Protein 4	AI	Proliferation		
SRSF8	Serine And Arginine Rich Splicing Factor 8	AI	Transcription	Y	
TMCC2	Transmembrane And Coiled-Coil Domain Family 2	AI	Metabolism	Y	
TRIM4	Tripartite Motif Containing 4	AI	Immune		
TWF2	Twinfilin Actin Binding Protein 2	AI	Actin and ATP Binding Site		
VTA1	Vesicle Trafficking 1	AI	Vesicle		
ZNF484	Zinc Finger Protein 484	AI	Transcription		

Table 6. Unique genes identified in SEVs isolated from COVID-19 cases
SEVs isolated from COVID-19 cases carry transcripts that are absent in Controls. The listed transcripts are not detected in SEVs isolated from Controls but are present in most samples in the identified COVID-19 groups. The cellular function, expression in trophoblasts, and pregnancy associated expression of each transcript is listed as well.

Control v. R1						
Upstream Regulator of Placenta Transcriptome					EV Expression	
gene symbol	**gene name**	**activation score**	**p-value**	**# targets**	**LEV**	**SEV**
IGF2	Insulin Like Growth Factor 2	1.96	2.41E-05	4	N	Y
JUN	Jun proto-oncogene	nc	4.74E-07	7	Y*	Y
UCP3	Uncoupling Protein 3	nc	9.82E-06	2	N	N
FOS	Fos proto-oncogene	nc	2.01E-05	6	Y	Y
P2RY1	Purinergic Receptor P2Y1	nc	2.06E-05	2	N	N
PRLH	Prolactin Releasing Hormone	nc	2.06E-05	2	N	N
FGF3	Fibroblast Growth Factor 3	nc	3.52E-05	2	N	N
LEPR	Leptin Receptor	nc	4.13E-05	4	Y	Y
GPX8	Glutathione Peroxidase 8 (Putative)	nc	4.40E-05	2	N	N
ELN	Elastin	nc	6.45E-05	2	N	N
LGALS1	Galectin 1	nc	8.82E-05	3	Y	Y
FGF19	Fibroblast Growth Factor 19	nc	9.77E-05	3	N	N
PER2	Period Circadian Regulator 2	nc	1.02E-04	2	N	N
USP38	Ubiquitin Specific Peptidase 38	nc	1.02E-04	2	N	N
FOXC2	Forkhead Box C2	nc	1.04E-04	3	N	N
PRKN	Parkin RBR E3 Ubiquitin Protein Ligase	nc	1.11E-04	3	N	Y
RARG	Retinoic Acid Receptor Gamma	nc	1.15E-04	3	N	N
GAL	Galanin And GMAP Prepropeptide	nc	1.33E-04	2	N	N
CD36	CD36 Molecule	nc	1.60E-04	3	Y	Y
PER1	Period Circadian Regulator 1	nc	2.04E-04	2	N	N
Control v. R3						
Upstream Regulator of Placenta Transcriptome					EV Expression	
gene symbol	**gene name**	**activation score**	**p-value**	**# targets**	**LEV**	**SEV**
TNF	Tumor Necrosis Factor	1.34	2.49E-05	16	N	N
CYP19A1	Cytochrome P450 Family 19 Subfamily A Member 1	0.882	1.52E-04	4	N	N
IL1B	Interleukin 1 Beta	-0.02	1.27E-04	11	Y^{+}	Y
ESR1	Estrogen Receptor 1	-0.27	4.36E-05	13	N	Y
PGR	Progesterone Receptor	-1.12	1.08E-05	7	N	N
AKT1	AKT Serine/Threonine Kinase 1	-1.42	1.03E-05	7	N	Y
AGT	Angiotensin	-1.44	9,92E-05	10	N	N
PPARG	Peroxisome Proliferator Activated Receptor Gamma	-1.63	4.27E-05	8	N	N
HIF1A	Hypoxia Inducible Factor 1 Subunit Alpha	-1.81	7.57E-05	8	Y	Y
TP53	Tumor Protein P53	-1.9	8.31E-05	15	N	Y
FASLG	Fas Ligand	nc	7.57E-06	4	N	N
SPZ1	Spermatogenic Leucine Zipper 1	nc	1.94E-05	3	N	Y
CXCR4	C-X-C Motif Chemokine Receptor 4	nc	2.16E-05	4	Y	N
PLD1	Phospholipase D1	nc	5.25E-05	3	N	N
IGF2	Insulin Like Growth Factor 2	nc	6.81E-05	5	Y	Y
ANGPTL6	Angiopoietin Like 6	nc	9.25E-05	2	N	N
MAP2K1	Mitogen-Activated Protein Kinase Kinase 1	nc	1.36E-04	5	N	N
PCBP1	Poly(RC) Binding Protein 1	nc	1.72E-04	2	Y	Y
IRS2	Insulin Receptor Substrate 2	nc	1.85E-04	3	N	Y
TRIM29	Tripartite Motif Containing 29	nc	2.21E-04	2	N	N

Control v. AI						
Upstream Regulator of Placenta Transcriptome					EV Expression	
gene symbol	**gene name**	**activation score**	**p-value**	**# targets**	**LEV**	**SEV**
FAS	Fas Cell Surface Death Receptor	1.46	5.86E-12	33	Y	N
GRN	Granulin Precursor	1.39	3.73E-12	19	Y	Y
EZH2	enhancer of zeste 2 polycomb repressive complex 2 subunit	1.04	1.15E-12	36	N	N
HRAS	HRas Proto-Oncogene, GTPase	0.67	3.72E-11	45	N	N
AHR	aryl hydrocarbon receptor	0.53	1.16E-11	38	N	N
CEBPB	CCAAT enhancer binding protein beta	0.35	4.92E-13	45	N	N
JUN	Jun proto-oncogene	0.04	3.54E-12	39	N	Y
STAT6	Signal Transducer and Activator of Transcription 6	-0.07	6.20E-14	40	N	N
IL13	Interleukin 13	-0.91	6.95E-19	47	N	N
TNF	Tumor Necrosis Factor	-0.98	6.17E-21	110	N	N
IL6	Interleukin 6	-1.34	7.28E-16	58	N	N
STAT3	Signal Transducer and Activator of Transcription 3	-2.07	4.88E-13	50	N	Y
IL10	Interleukin 10	-2.15	2.74E-17	45	N	N
IL1B	Interleukin 1 Beta	-2.21	5.16E-16	71	Y	Y
IL4	Interleukin 4	-2.36	6.94E-20	81	N	N
IGF1	Insulin Like Growth Factor 1	-2.37	1.28E-11	42	N	Y
MAFB	MAF BZIP Transcription Factor B	-3.02	3.53E-11	16	N	N
IFNG	Interferon Gamma	-4.00	1.27E-16	86	N	Y
TGFB1	Transforming Growth Factor Beta 1	-4.56	2.01E-23	115	N	N
AGT	Angiotensinogen	-4.74	1.26E-18	67	N	Y

Table 7. Placenta RNAseq upstream regulators
Ingenuity pathway analysis predicted upstream regulators of transcriptional changes in COVID-19 placenta compared to control. The activation score, p-value and number of targets identified in the dataset are listed for the top 20 predicted biological upstream regulators. Expression of the same gene in large and small EVs is recorded. An asterisk identifies instances where the differential gene expression between Control and the COVID-19 group is statistically different ($p<0.05$). A plus sign identifies a statistical difference of $p<0.1$.

Control v. R1 Placenta Transcriptome			
gene symbol	**gene name**	**FC**	**adj p-value**
GS1-600G8.3	unknown	7.48	2.09E-04
AC027288.3	unknown	6.85	4.35E-04
RORB	RAR Related Orphan Receptor B	6.10	3.45E-05
MMP12	Matrix Metallopeptidase 12	5.20	2.22E-04
OMD	Osteomodulin	4.32	3.48E-03
IGFBP6	Insulin Like Growth Factor Binding Protein 6	2.40	7.81E-05
UPK1B	Uroplakin 1B	2.59	1.16E-05
FN1	Fibronectin 1	2.38	1.41E-06
SDK1	Sidekick Cell Adhesion Molecule 1	1.62	1.15E-04
MTARC2	Mitochondrial Amidoxime Reducing Component 2	-2.15	1.67E-05
Control v. R2 Placenta Transcriptome			
gene symbol	**gene name**	**FC**	**adj p-value**
SCN9A	Sodium Voltage-Gated Channel Alpha Subunit 9	-1.70	0.047
MAP1LC3C	Microtubule Associated Protein 1 Light Chain 3 Gamma	-3.37	0.008
Control v. R3 Placenta Transcriptome			
gene symbol	**gene name**	**FC**	**adj p-value**
AC079777.1	Unknown	6.12	4.31E-03
STAT4	Signal Transducer and Activator of Transcription 4	3.04	1.14E-03
ADARB1	Adenosine Deaminase RNA Specific B1	-1.77	1.08E-03
MICAL3	Microtubule Associated Monooxygenase, Calponin and LIM Domain Containing 3	-1.97	8.89E-06
SYNPO2	Synaptopodin 2	-2.37	5.27E-03
SIGLEC6	Sialic Acid Binding Ig Like Lectin 6	-2.46	1.37E-04
PRELP	Proline And Arginine Rich End Leucine Rich Repeat Protein	-2.52	1.64E-03
ENO2	Enolase 2	-3.13	4.69E-06
MEG9	Maternally Expressed 9	-3.52	4.31E-03
MAP1LC3C	Microtubule Associated Protein 1 Light Chain 3 Gamma	-3.80	1.37E-04
Control v. AI Placenta Transcriptome			
gene symbol	**gene name**	**FC**	**adj p-value**
PRL	Prolactin	6.30	6.45E-08
PENK	Proenkephalin	5.10	1.84E-05
TMPRSS3	Transmembrane Serine Protease 3	3.83	3.94E-08
GNLY	Granulysin	3.39	2.08E-05
LAMB3	Laminin Subunit Beta 3	2.99	2.40E-06
SLC22A3	Solute Carrier Family 22 Member 3	-2.16	2.45E-05
BMP5	Bone Morphogenetic Protein 5	-2.56	2.42E-05
CLIC2	Chloride Intracellular Channel 2	-2.67	2.04E-05
P2RX1	Purinergic Receptor P2X 1	-3.42	1.23E-05
PTGER2	Prostaglandin E Receptor 2	-3.45	1.33E-05

Supplemental Table 1. Placenta RNAseq DEG
Differentially expressed genes (DEG) were identified by comparing COVID-19 groups to controls. The top 10 DEGs are reported with the log 2-fold change (FC) and adjusted p-value. When comparing R2 to control, only 2 genes surpassed the thresholds.

Uniquely Expressed Transcripts Associated with Adverse Pregnancy Outcomes					
Gene Symbol	**Gene Name**	**EV Population**	**Uniquely Expressed in Group(s)**	**No Expression in Group(s)**	**Adverse Pregnancy Outcome(s)**
CENPT	Centromere Protein T	LEV	Control	R1	FGR(*95*)
IMP3	IMP U3 Small Nucleolar Ribonucleoprotein 3	SEV	Control	R1	PE (*96*)
RAP1GDS1	Rap1 GTPase-GDP Dissociation Stimulator 1	LEV	Control	R2	FGR (*97*)
LRRC8B	Leucine Rich Repeat Containing 8 VRAC Subunit B	LEV	Control	R2	PTB (*98*)
RNF138	Ring Finger Protein 138	LEV	Control	R2	FGR (*97*)
APPL1	Adaptor Protein, Phosphotyrosine Interacting with PH Domain And Leucine Zipper 1	LEV	Control	R2	FGR (*99*)
PAFAH1B2	Platelet Activating Factor Acetylhydrolase 1b Catalytic Subunit 2	LEV	Control	R2	PE, gHTN, FGR (*100, 101*)
CCDC18	Coiled-Coil Domain Containing 18	LEV	Control	R2	PE (*102*)
RNASE1	Ribonuclease A Family Member 1, Pancreatic	SEV	Control	R2	PE (*103*)
METTL14	Methyltransferase 14, N6-Adenosine-Methyltransferase Subunit	LEV	Control	R3	PE (*104, 105*)
LIN54	Lin-54 DREAM MuvB Core Complex Component	LEV	Control	R3	FGR (*106*)
FPR2	Formyl Peptide Receptor 2	LEV	Control	R3	FGR (*107*)
ALDH1A1	Aldehyde Dehydrogenase 1 Family Member A1	LEV	Control	R3	FGR (*108*)
S1PR4	Sphingosine-1-Phosphate Receptor 4	LEV	Control	AI	PE (*109*)
THAP12	THAP Domain Containing 12	LEV	Control	AI	FGR (*97*)
TNFSF13	TNF Superfamily Member 13	LEV	Control	AI	PE (*110*)
PSG2	Pregnancy Specific Beta-1-Glycoprotein 2	LEV	Control	R2, AI	PE, PTB, FGR (*111-113*)
APBA3	Amyloid Beta Precursor Protein Binding Family A Member 3	LEV	Control	R2, R3, AI	PE (*114*)
MXD1	MAX Dimerization Protein 1	LEV	R1	Control	PTB (*115*) PE (*116*)

RYBP	RING1 And YY1 Binding Protein	LEV	R1	Control	PE (*117-119*)
A2M	Alpha-2-Macroglobulin	LEV	R1	Control	PE (*120*) PTB (*121*)
HK1	Hexokinase 1	LEV	R1	Control	PE (*122*)
CAPG	Capping Actin Protein, Gelsolin Like	SEV	R2	Control	PE (*123*) PTB (*124*)
SLC1A5	Solute Carrier Family 1 Member 5	SEV	R2	Control	PE (*91*)
XRN1	5'-3' Exoribonuclease 1	LEV	AI	Control	PE (*125*)
WDR26	WD Repeat Domain 26	LEV	AI	Control	FGR (*97*)
GPBP1L1	GC-Rich Promoter Binding Protein 1 Like 1	LEV	AI	Control	FGR (*106*)
FOXP1	Forkhead Box P1	LEV	AI	Control	PE (*126*)
NEAT1	Nuclear Paraspeckle Assembly Transcript 1	LEV	AI	Control	PE (*127*) FGR (*128*)
KIF5B	Kinesin Family Member 5B	SEV	AI	Control	PE (*129*)
CSNk2B	Casein Kinase 2 Beta	SEV	AI	Control	FGR (*130*)
MYLK	Myosin Light Chain Kinase	SEV	AI	Control	PE (*116, 131*)
HSP90B1	Heat Shock Protein 90 Beta Family Member 1	SEV	AI	Control	PE (*132*) PTB (*133*)
MUC22	Mucin 22	SEV	AI	Control	FGR (*134*)
GRHL1	Grainyhead Like Transcription Factor 1	SEV	AI	Control	FGR (*135*)
SHC4	SHC Adaptor Protein 4	SEV	AI	Control	PE (*136*)
CTSS	Cathepsin S	SEV	R3, AI	Control	FGR (*137*)

Supplemental Table 2. EV Transcripts Associated with Adverse Pregnancy Outcomes
Many transcripts detected in EVs are previously reported to be differentially expressed in adverse pregnancy complications. The gene, EV subpopulation (small [SEV] or large [LEV] EVs), unique expression, and identified literature are listed in the table.

Figure 1

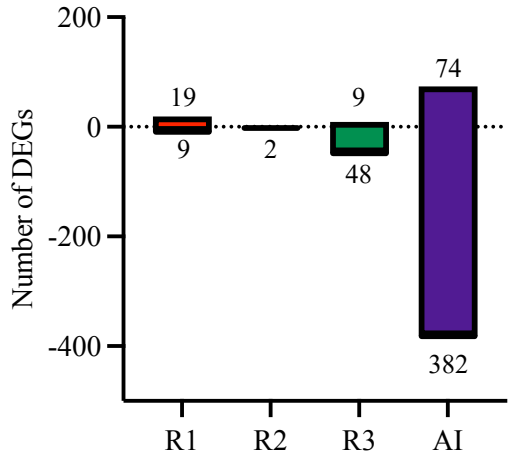

Figure 2

A

Large EV

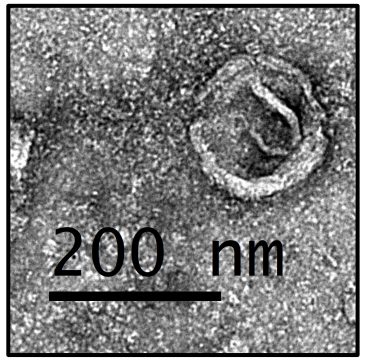

Small EV

B

Large EVs

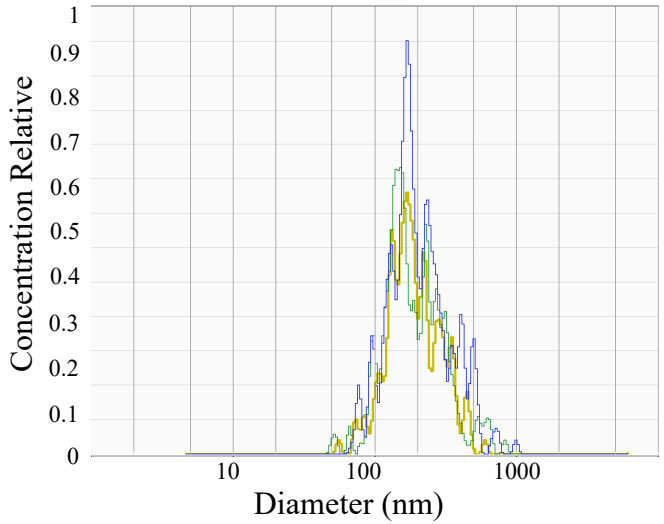

Small EVs

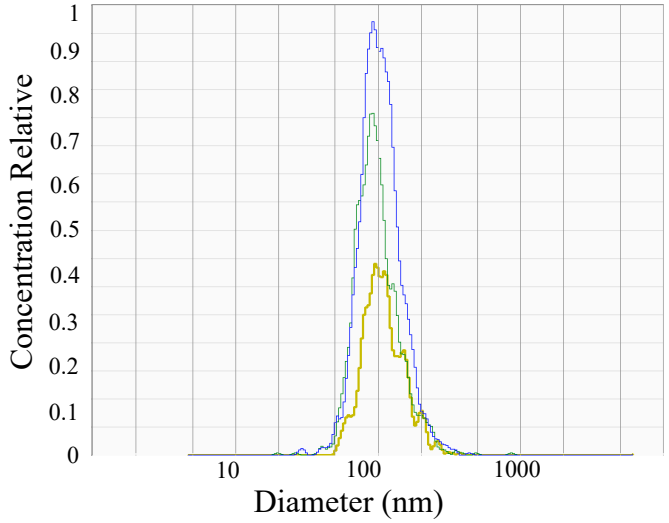

C

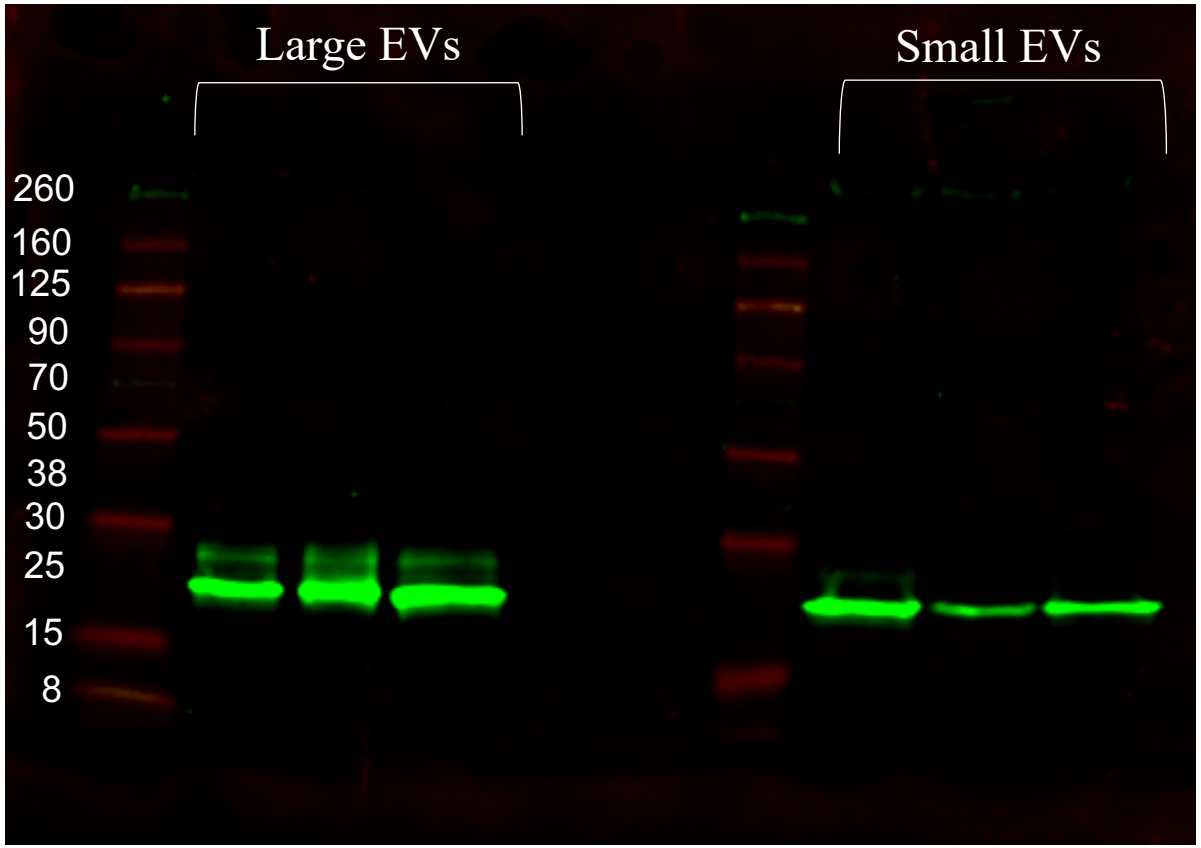

Figure 3

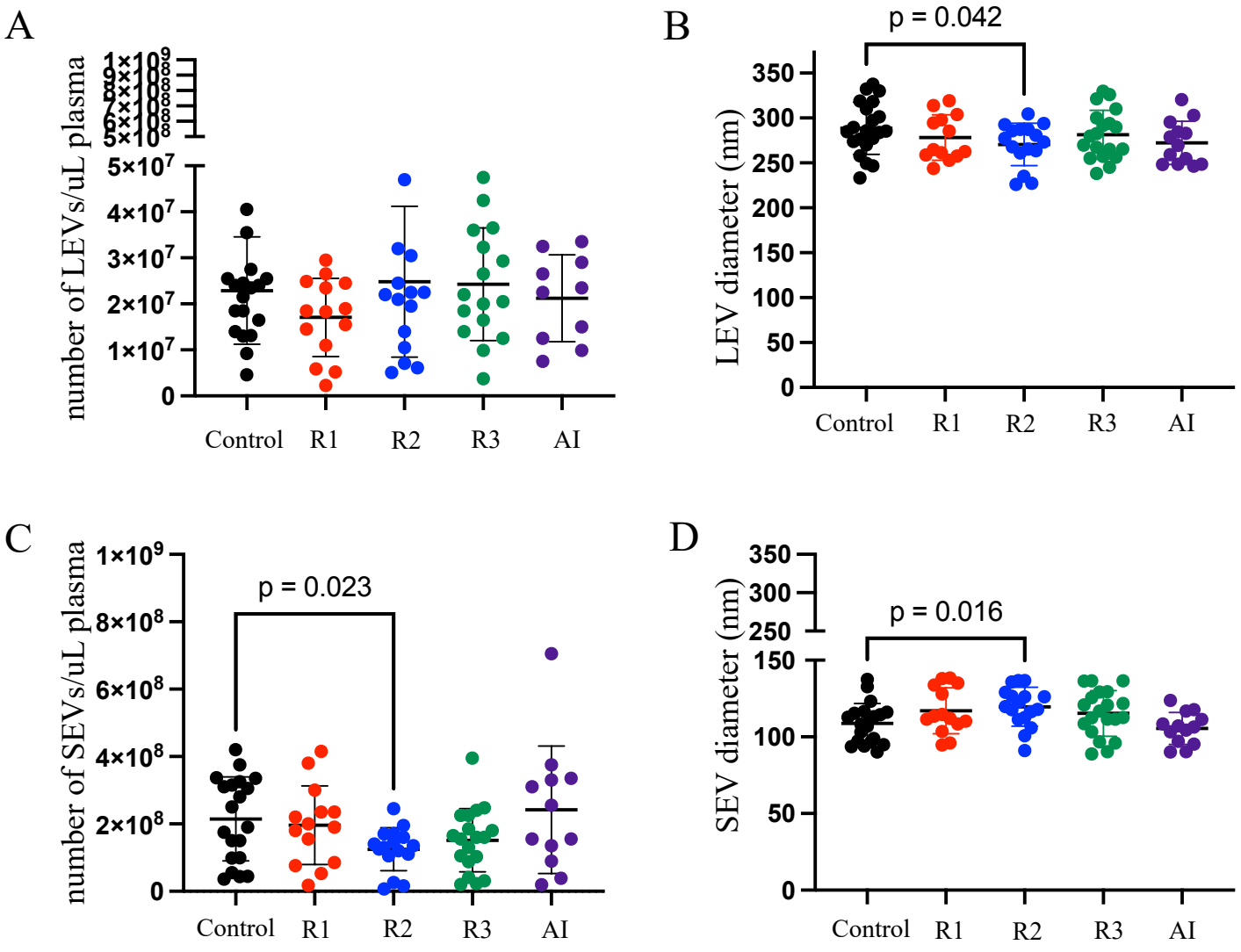
A
number of LEVs/uL plasma
1×10^9
9×10^8
8×10^8
7×10^8
6×10^8
5×10^8
5×10^7
4×10^7
3×10^7
2×10^7
1×10^7
0
Control
R1
R2
R3
AI
B
p = 0.042
LEV diameter (nm)
350
300
250
200
150
100
50
0
Control
R1
R2
R3
AI
C
number of SEVs/uL plasma
p = 0.023
1×10^9
8×10^8
6×10^8
4×10^8
2×10^8
0
Control
R1
R2
R3
AI
D
SEV diameter (nm)
p = 0.016
350
300
250
150
100
50
0
Control
R1
R2
R3
AI

Figure 4

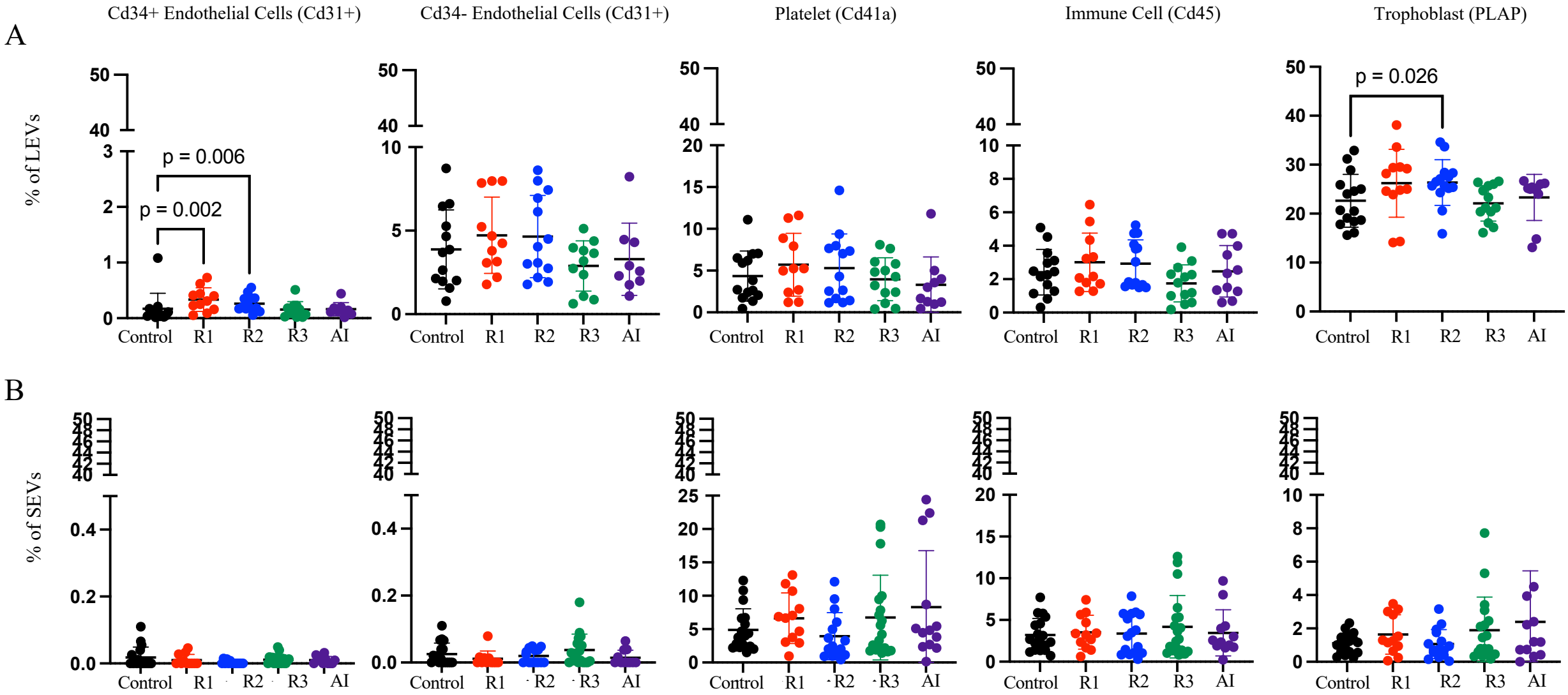
A
Cd34+ Endothelial Cells (Cd31+)
Cd34- Endothelial Cells (Cd31+)
Platelet (Cd41a)
Immune Cell (Cd45)
Trophoblast (PLAP)
% of LEVs
p = 0.006
p = 0.002
p = 0.026
Control
R1
R2
R3
AI
B
% of SEVs

Figure 5

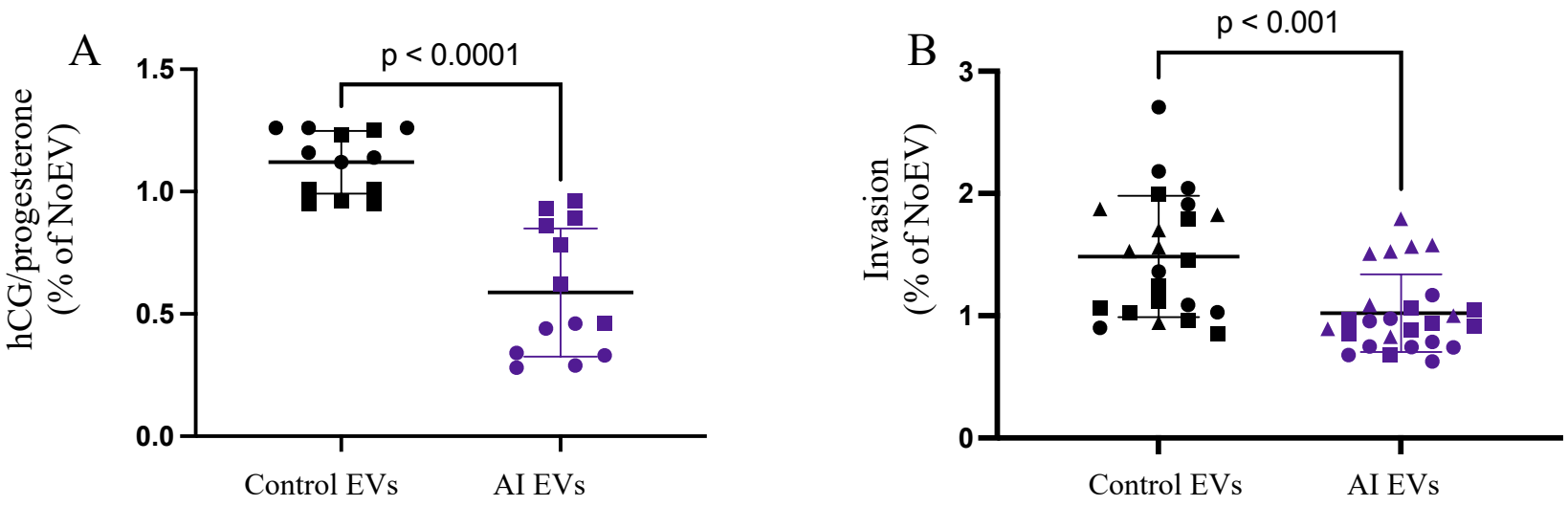
A
p < 0.0001
hCG/progesterone
(% of NoEV)
1.5
1.0
0.5
0.0
Control EVs
AI EVs
B
p < 0.001
Invasion
(% of NoEV)
3
2
1
0
Control EVs
AI EVs

Figure 6

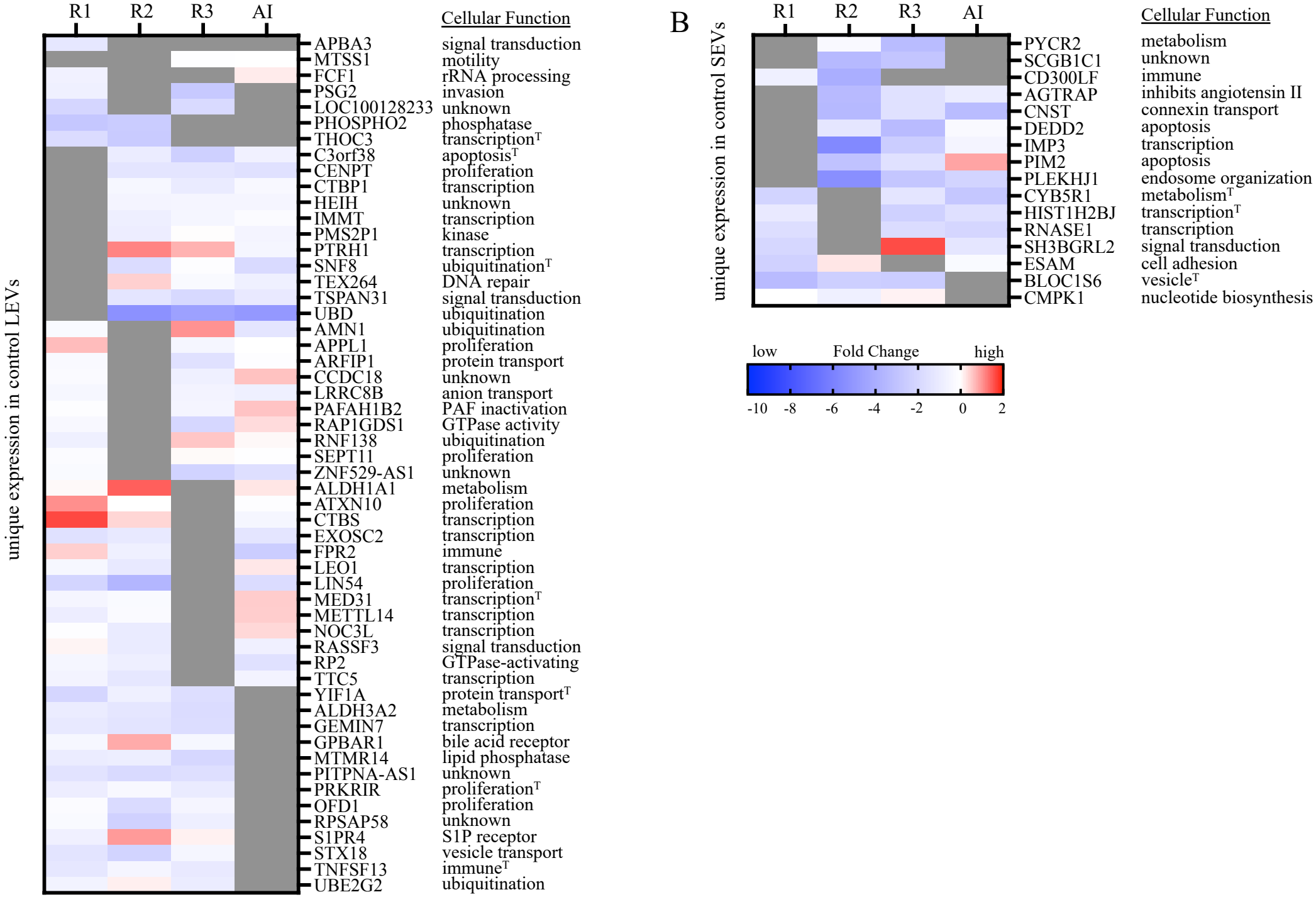
A
R1
R2
R3
AI
unique expression in control LEVs
Cellular Function
APBA3 signal transduction
MTSS1 motility
FCF1 rRNA processing
PSG2 invasion
LOC100128233 unknown
PHOSPHO2 phosphatase
THOC3 transcriptionT
C3orf38 apoptosisT
CENPT proliferation
CTBP1 transcription
HEIH unknown
IMMT transcription
PMS2P1 kinase
PTRH1 transcription
SNF8 ubiquitinationT
TEX264 DNA repair
TSPAN31 signal transduction
UBD ubiquitination
AMN1 ubiquitination
APPL1 proliferation
ARFIP1 protein transport
CCDC18 unknown
LRRC8B anion transport
PAFAH1B2 PAF inactivation
RAP1GDS1 GTPase activity
RNF138 ubiquitination
SEPT11 proliferation
ZNF529-AS1 unknown
ALDH1A1 metabolism
ATXN10 proliferation
CTBS transcription
EXOSC2 transcription
FPR2 immune
LEO1 transcription
LIN54 proliferation
MED31 transcriptionT
METTL14 transcription
NOC3L transcription
RASSF3 signal transduction
RP2 GTPase-activating
TTC5 transcription
YIF1A protein transportT
ALDH3A2 metabolism
GEMIN7 transcription
GPBAR1 bile acid receptor
MTMR14 lipid phosphatase
PITPNA-AS1 unknown
PRKRIR proliferationT
OFD1 proliferation
RPSAP58 unknown
S1PR4 S1P receptor
STX18 vesicle transport
TNFSF13 immuneT
UBE2G2 ubiquitination
B
R1
R2
R3
AI
unique expression in control SEVs
Cellular Function
PYCR2 metabolism
SCGB1C1 unknown
CD300LF immune
AGTRAP inhibits angiotensin II
CNST connexin transport
DEDD2 apoptosis
IMP3 transcription
PIM2 apoptosis
PLEKHJ1 endosome organization
CYB5R1 metabolismT
HIST1H2BJ transcriptionT
RNASE1 transcription
SH3BGRL2 signal transduction
ESAM cell adhesion
BLOC1S6 vesicleT
CMPK1 nucleotide biosynthesis
low
Fold Change
high
-10 -8 -6 -4 -2 0 2

Figure 7

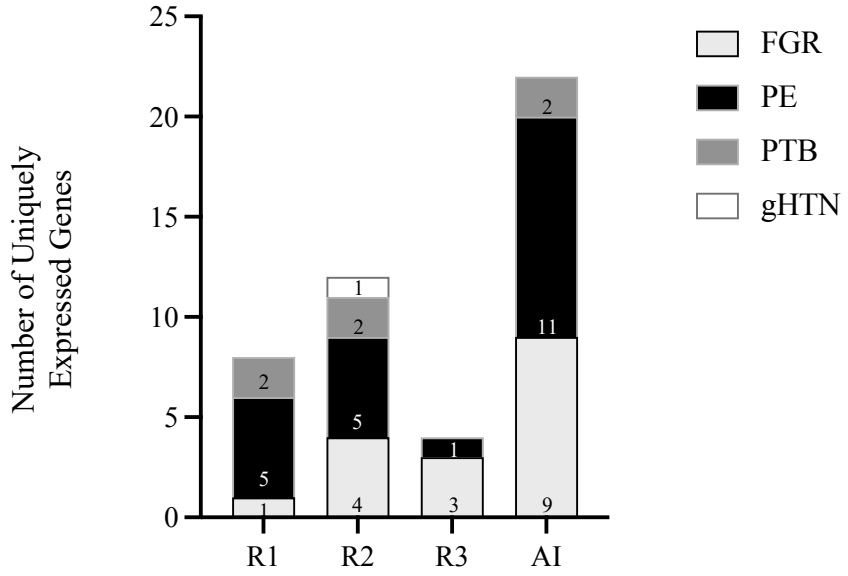
Number of Uniquely Expressed Genes
25
20
15
10
5
0
R1
R2
R3
AI
FGR
PE
PTB
gHTN
2
5
1
1
2
5
4
1
3
2
11
9

Figure 8

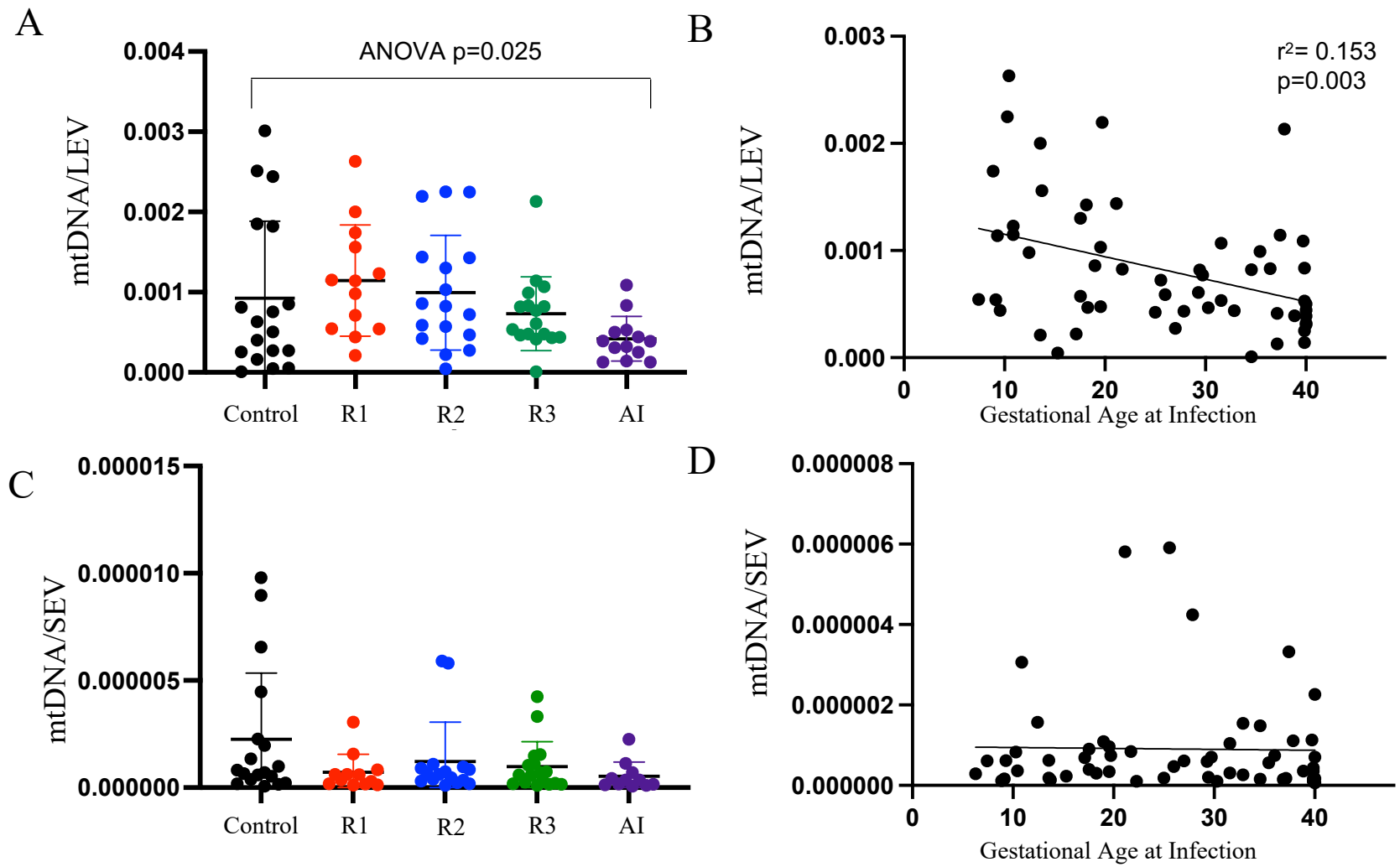
A
ANOVA p=0.025
mtDNA/LEV
0.004
0.003
0.002
0.001
0.000
Control
R1
R2
R3
AI
B
r²= 0.153
p=0.003
mtDNA/LEV
0.003
0.002
0.001
0.000
0
10
20
30
40
Gestational Age at Infection
C
mtDNA/SEV
0.000015
0.000010
0.000005
0.000000
Control
R1
R2
R3
AI
D
mtDNA/SEV
0.000008
0.000006
0.000004
0.000002
0.000000
0
10
20
30
40
Gestational Age at Infection